

**REMOTE SENSING BASED
HYDROLOGICAL MODELLING
FOR FLOOD EARLY WARNING
IN THE UPPER AND MIDDLE
AWASH RIVER BASIN**

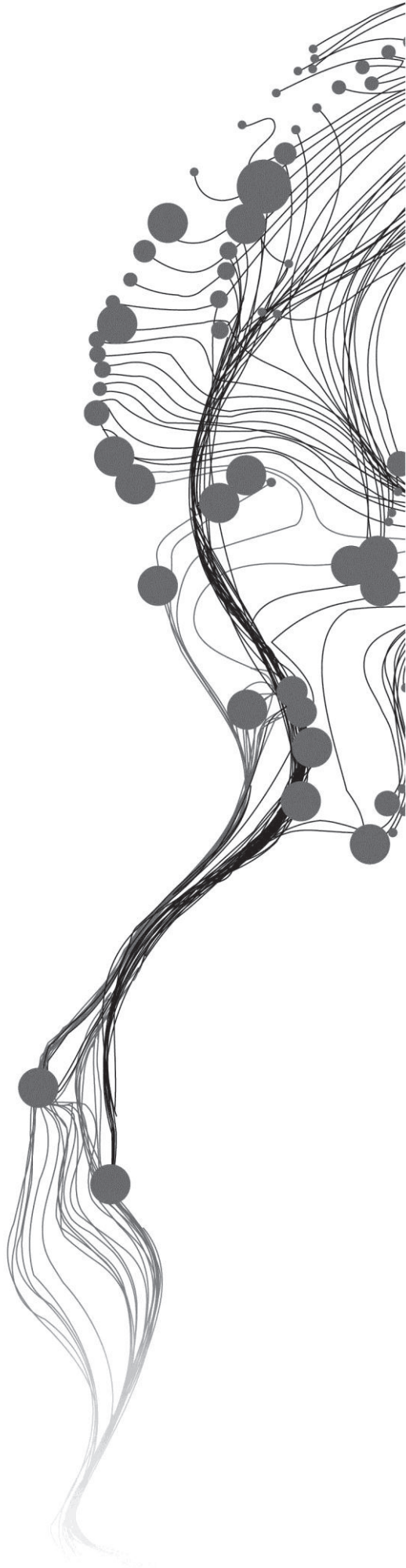
SIFAN ABERA KORICHE

March, 2012

SUPERVISORS:

Dr.Ing. T.H.M. Tom Rientjes

Dr. B.H.P. Ben Maathuis



REMOTE SENSING BASED HYDROLOGICAL MODELLING FOR FLOOD EARLY WARNING IN THE UPPER AND MIDDLE AWASH RIVER BASIN

SIFAN ABERA KORICHE

Enschede, The Netherlands, March, 2012

Thesis submitted to the Faculty of Geo-Information Science and Earth Observation of the University of Twente in partial fulfilment of the requirements for the degree of Master of Science in Geo-information Science and Earth Observation.

Specialization: Water Resources and Environmental Management

SUPERVISORS:

Dr. Ing. T.H.M. Tom Rientjes

Dr. B.H.P. Ben Maathuis

THESIS ASSESSMENT BOARD:

Prof. Dr. Z. (Bob) Su (Chair)

Dr. Muktar Reshid (External Examiner, UN-World Food Program, Ethiopia)

Dr. Ing. T.H.M. Tom Rientjes

Dr. B.H.P. Ben Maathuis

DISCLAIMER

This document describes work undertaken as part of a programme of study at the Faculty of Geo-Information Science and Earth Observation of the University of Twente. All views and opinions expressed therein remain the sole responsibility of the author, and do not necessarily represent those of the Faculty.

ABSTRACT

Floods often have an enormous impact on the environment and society. In addition to the tragic loss of life, the impacts of floods include damage to property and environment and the loss of livelihood. In Ethiopia, flood disasters are attributed to rivers that overflow or burst their banks and inundate downstream plain lands. A major river basin that has serious flood problems is the Awash River Basin that is largely located in the Rift Valley. In order to prevent impacts of floods, an early warning system is a prerequisite. This study serves to evaluate if a flood early warning system for the upper and middle Awash River Basin located in Ethiopia could be developed by applying remote sensing based hydrological modelling. Satellite derived products from GEONETCast, National Oceanic and Atmospheric Administration Climate Prediction Centre (NOAA CPC) and Famine Early Warning System Network (FEWS NET) data streams were used to force the hydrological model (LISFLOOD); and the results were compared with observations of river discharge in the area. The model was calibrated by trial and error using observed stream flow from 2007 and 2008 and validated using 2009. The sensitivity of five model parameters was performed to evaluate and assess the LISFLOOD model performance in simulating the upper and middle Awash River flow. Furthermore, integrated index maps, which indicate source areas for flooding were produced by combining the standard precipitation index (SPI) and the topographic wetness index (TWI). In addition, an attempt was made to validate the satellite derived soil moisture product (MetOp-ASCAT-12.5km) using in-situ soil moisture measurements. According to the result from the sensitivity analysis, two LISFLOOD model parameters (LZTC and GWPV) affected the base flow part of the hydrograph, whereas, the effects of the other three parameters (UZTC, PPBF and Xb) are on the quick flow. For the calibration period RMSE = 55.29m³s⁻¹, NSE = 0.72 and RVe = 0.27% and for validation period RMSE = 29.37m³s⁻¹, NSE = 0.82 and RVe = 21.07% were obtained. From the analysis of daily SPI of the wet period, two windows of time (June 13 – 20 and July 27 – August 04) were found that have high SPI values (>1). The two windows of time indicate the periods that the rainfall occurs may cause flooding in flood prone areas. The combined index analysis illustrated the spatial distribution of possible source areas for floods in the flood prone areas.

Keyword: LISFLOOD, Standard Precipitation Index (SPI), Topographic Wetness Index (TWI) Early warning, Flood

ACKNOWLEDGEMENTS

This thesis would not have been possible without the guidance and the help of several individuals who in one way or another contributed and extended their valuable assistance in the preparation and completion of this study. In fact, it is almost impossible to list all of them, and therefore the following list is horribly incomplete. However, it would be worse not to make an attempt to acknowledge those who have played a key role in the research work.

First and foremost, I gratefully acknowledge the contributions of my first supervisor, Dr. Ing. T.H.M. Tom Rientjes, whose patience, dedication, and knowledge guided me through the thesis work, it was a great pleasure to work with him. I would like to extend my acknowledgement to my second supervisor Dr. B.H.P. Ben Maathuis for guiding and reviewing my work and helping me in getting data. Furthermore, it is a pleasure to thank those who made the fieldwork in Ethiopia possible: Dr. Muktar Reshid, Mr. Kassa Fekadu and Mrs. Almaz Demessie.

My acknowledgement also goes to the Netherlands Fellowship Program (NFP) for funding my studies and this research.

Last but not least, I pass my regards and blessings to all my family, friends and the one above all, the Almighty God, for answering my prayers and for giving me the strength to finish this thesis work. Thank you so much my dear Lord.

TABLE OF CONTENTS

Abstract	i
Acknowledgements	ii
Table of contents	iii
List of figures	v
List of tables	vi
1. Introduction	1
1.1. Background	1
1.2. Statement of problem	2
1.3. Objectives and research questions	2
1.3.1. Main objective	2
1.3.2. Specific objectives	2
1.3.3. Research questions	2
1.4. Outline of the thesis	3
2. Literature Review	5
2.1. Flood early warning	5
2.2. Rainfall runoff model selection	6
2.3. LISFLOOD model	7
2.3.1. Introduction	7
2.3.2. Previous studies	8
2.4. GEONETCast	9
3. Study area and data sets	11
3.1. Study area	11
3.2. Data Sets	12
3.2.1. Data from offices	13
3.2.2. Satellite data products	15
3.2.3. In-situ measured data	16
4. Research method	17
4.1. Introduction	17
4.2. Data preprocessing	18
4.2.1. Rainfall data	18
4.2.2. Potential Evapotranspiration	19
4.2.3. Leaf Area Index	21
4.2.4. Land cover and soil type	22
4.2.5. Digital Elevation Model	22
4.3. Model setup	24
4.3.1. Model input files (parameters)	25
4.3.2. The settings file	26
4.3.3. Output generated by the LISFLOOD	27
4.4. Initialization of the model	27
4.5. Model calibration	28
4.6. ASCAT surface soil moisture	29
4.7. Flood prone area(s) verification using water level simulation in LISFLOOD	29
4.8. Standardized Precipitation Index	30

4.9. Topographic Wetness Index	31
4.10. Combining SPI and TWI	31
5. Result and Discussion	33
5.1. Reference evapotranspiration (ET _o) analysis	33
5.2. Rainfall data analysis and comparison	34
5.3. Selection of observed hydrograph for model calibration and validation	36
5.4. Sensitivity analysis of LISFLOOD input parameters	38
5.4.1. Effects of the Lower Zone Time Constant (LZTC) parameter	39
5.4.1.1. Effects of the Groundwater Percolation Value (GWPV) Parameter	39
5.4.1.2. Effects of the Upper Zone Time Constant (UZTC) parameter	40
5.4.1.3. Effects of the Power Preferential Bypass Flow (PPBF) parameter	40
5.4.1.4. Effect of Xinanjiang parameter 'b' (X _b)	41
5.5. Calibration and validation results	41
5.6. Simulation result using FEWS NET and in-situ based ET _o	42
5.7. Water level simulation for flood prone area(s) verification and onset of flooding	43
5.8. ASCAT surface soil moisture to identify the wet pixel	43
5.9. Analysis for Combining SPI and TWI	45
5.10. Relation between water level and peak flow with SPI	47
6. Conclusions and Recommendations	49
6.1. Summary and Conclusions	49
6.2. Recommendations	51
List of references	53
Annex	57

LIST OF FIGURES

Figure 2-1: Schematic representation of LISFLOOD model without including snowmelt (Source: Van Der Knijff et al., 2008).....	8
Figure 2-2: GEONETCast system overview (EUMETSAT, October 2007).....	10
Figure 2-3: GEONETCast toolbox version 1.3 menu (source: plug-in with in ILWIS software).....	10
Figure 3-1: Location map of the study area.....	11
Figure 3-2: Longitudinal Section of Awash River Channel (Source: Halcrow, 2006)	12
Figure 3-3: Meteorological and Hydrological stations in the study area.....	13
Figure 3-4: Observed stream flow hydrograph of selected 6 stations.....	14
Figure 3-5: Soil type and land cover of the study area (source: Awash Basin Authority, after Halcrow, 2006)	15
Figure 3-6: Sample sites for surface soil moisture measurement and photographs taken during field visit	16
Figure 4-1: Flow chart of the research method	17
Figure 4-2: Command line syntax of the script used to convert CMORPH rainfall ILWIS raster format to PCRaster time series maps of rainfall.....	19
Figure 4-3: Local drain direction	24
Figure 4-4: Geometry of channel cross-section (Source: Van Der Knijff and De Roo, 2008).....	30
Figure 4-5: Flowchart for combining SPI and TWI	31
Figure 5-1: (a) Daily variation of FEWS NET and <i>in-situ</i> based ETo estimates at Bishoftu station (2006 – 2007) and (b) annual FEWS NET and <i>in-situ</i> based ETo estimates at respective station for the year 2007	34
Figure 5-2: CMORPH and station rainfall data comparison.....	35
Figure 5-3: MPE and station rainfall data comparison.....	35
Figure 5-4: Double mass curve of cumulative observed discharge vs. satellite rainfall.....	37
Figure 5-5: Observed stream flow at Melka Hombole station used for calibration and validation of the model.....	37
Figure 5-6: Sub catchments for which the double mass curve analysis was applied	37
Figure 5-7: Sensitivity of the model to change in Lower Zone Time Constant parameter.....	39
Figure 5-8: Sensitivity of the model to changes in the Groundwater Percolation Value parameter.....	39
Figure 5-9: Sensitivity of the model to changes in the Upper Zone Time Constant parameter.....	40
Figure 5-10: Sensitivity of the model to changes in the Power Preferential Bypass Flow parameter.....	41
Figure 5-11: Sensitivity of the model to changes in the Xinanjiang parameter 'b'.....	41
Figure 5-12: Simulated and Observed hydrograph for the period 2007 – 2009 at Melka Hombole gauge station	42
Figure 5-13: Comparison between observed and simulated hydrograph using FEWS NET and <i>in-situ</i> based ETo	42
Figure 5-14: Water level simulation at the flood prone areas.....	43
Figure 5-15: Soil moisture validation result at Mojo area (a) and sample sites (b).....	44
Figure 5-16: ASCAT surface soil moisture a) May 13, 2008; b) July 31, 2008; and c) July 7, 2008 day time overpasses	44
Figure 5-17: Locations where the SPI values of the wet season (June – August) were taken.....	45
Figure 5-18: Temporal variation of wet season SPI: a) 1 st site, b) 2 nd site and c) 3 rd site	45
Figure 5-19: Combined index of 2007: a) window one and b) window two	46

LIST OF TABLES

Table 2-1: Flood forecasting and early warning initiatives in Africa (After Thieming et al., 2011)	5
Table 2-2: Some of the global and continental flood monitoring and early warning systems (This work)	6
Table 3-1: Meteorological and Hydrological stations in the study area	14
Table 3-2: Satellite products with their spatial and temporal resolutions, source and period of records	15
Table 4-1: The form of batch file used to convert ETo to EW0	21
Table 4-2: LISFLOOD input maps (after Van Der Knijff and De Roo, 2008)	25
Table 4-3: LISFLOOD input tables (after Van Der Knijff and De Roo, 2008)	26
Table 4-4: The basic structures of the setting file (after Van Der Knijff and De Roo, 2008)	26
Table 4-5: The default output from LISFLOOD simulation (after by Van Der Knijff and De Roo, 2008)	27
Table 4-6: Calibration parameters of the LISFLOOD model (Source: Feyen et al., 2007)	29
Table 4-7: Category of SPI (adapted from McKee et al., 1993)	30
Table 5-1: RMSE values at respective stations. RMSE for AMAK and ShDb were calculated using the average ETo at the respective stations	33
Table 5-2: Correction factor applied for the respective year	36
Table 5-3: Parameters and objective functions for sensitivity analysis	38
Table 5-4: Optimized parameter and objective function values for calibration and validation period	41

1. INTRODUCTION

1.1. Background

Disasters cause much misery, particularly in developing countries where there is poor management and protection of the environment due to low economic potential (WMO, 2009). According to reports from the World Meteorological Organization (2009) approximately 70% of all disasters occurring in the world are related to hydro-meteorological events. Among the disasters, flooding probably contributes to the greatest hazard. Floods often have an enormous impact on the environment and society. Despite the tragic loss of life, impacts of floods are damages to property, environment and loss of livelihood. In Ethiopia floods have been occurring at different places and times with varying magnitude. Floods disasters are attributed to rivers that overflow or burst their banks and inundate downstream plain lands. Particularly large scale flooding (riverine flooding) in the country is common in the lowland flat parts due to high intensity of rainfall from highland parts of the country (Taddese et al., 2006). A major river basin that has serious flood problems is the Awash River Basin (110,000 km²) with largest part located in the Rift Valley (Achamyeleh, 2003).

There is high variation in seasonal discharge of Awash River basin. Floodings along the river occur every year but extreme floodings have occurred in 1996, 1999 and 2003. Although the extent and losses of life and assets were not reported, the flood event of 1996 was reported as the most extreme one. The 1999 flood was so severe that the military force was called in to help. According to Guinand (1999) report, the flood destroyed about 9,500 ha of cropped farmland, affected a population of about 85,000 people. In 2003, rainfall for three consecutive days has caused flood inundation of 19,480 km² of land and over 7,000 people were forced out of their homes and hundreds of animals were swept away by the water (NASA, 2011). In order to prevent such kind of tragic loss, developing an early warning system is a prerequisite.

Currently, the Ethiopian Disaster Risk Management and Food Security Sector (DRMSS) of the Ministry of Agriculture and the National Meteorological Agency (NMA) in collaboration with UN World Food Program (UN-WFP) aim to set up an early warning assessment tool for water and food supply security (Mannaerts and Maathuis, 2011). In this initiative, software for drought indexing called LEAP (Livelihood Early Assessment Protection) was developed in 2006. The tool serves for drought early warning assessment and specifically designed for the local Ethiopian context (Hoefsloot, 2010). However, due to the limitation of the model for serving as flood early warning assessment, applying other method(s) and/or improving LEAP were among the options. In order to improve the spatial as well as temporal accuracies of the early warning assessments of LEAP, the Faculty of Geo-Information Science and Earth Observation at University of Twente is conducting a pilot project with UN-WFP in collaboration with the DRMFSS and NMA to implement the use of new and near real time GEONETCast data streams. This research thesis is part of the pilot project, which focus on development of a flood early warning systems using new and near real time data from GEONETCast data stream and coupling this with a hydrological model (flood model) and Geographical Information Systems (GIS).

Therefore, using GIS and physically based spatially distributed rainfall runoff model LISFLOOD, which is developed for simulating hydrological process that occur in catchments has an important role in flood early warning (De Roo et al., 2000). Most of the input data sets used for the model are satellite derived products.

1.2. Statement of problem

Water resource potential of Ethiopia is found abundantly. However, integrated water resource management is not in its advanced stage (Achamyeleh, 2003). As part of the management technique, flood risk alleviation by employing integrated research and development is not at a stage where it is supposed to be. There have been various initiatives to address the problem of flooding and hydrological processes in upper and middle Awash River Basin (Abraha, 2006; Alemayehu, 2007). In addition, the Awash River flood control study has been started in 2004, by funds from the World Development Bank Group (WDBG) and is still on-going (ADBG, 2011). In spite of the recurrent flood problem, the existing disaster management mechanism is primarily focused on strengthening rescue and relief arrangements during and after major flood disasters. Little work has been done in a scientific context on minimizing the incidence and extent of flood damage. This necessitates the development of a flood early warning system and/or decision tools, which relies on hydrological modelling and the use of near real time data available through GEONETCast.

The meteorological input data used for modelling to develop flood early warning system can be from field measurements (gauges) or from satellites. The problem with meteorological data from gauges has limited temporal and spatial coverage. Also, it only represents point measurements and does not provide complete coverage of processes that occur in a catchment. Hence, using (near real time) satellite derived products as an input to a model for developing flood early warning system has an advantage, because it provides good temporal and spatial coverage.

1.3. Objectives and research questions

1.3.1. Main objective

The main objective of this research is to evaluate if a flood early warning system for the upper and middle Awash River Basin located in Ethiopia could be developed by applying remote sensing based hydrological modelling. Such modelling is often claimed to be effective but not practiced in Awash River Basin.

1.3.2. Specific objectives

- To simulate the stream flow of the upper and middle Awash River Basin using LISFLOOD;
- To assess the sensitivity of the LISFLOOD model to parameter value changes and evaluate the accuracy;
- To simulate the daily Awash River water level in flood prone areas and identify periods of overtopping from the river channel;
- To validate the satellite derived soil moisture product (MetOp-ASCAT-12.5km) using *in-situ* soil moisture measurements;
- To develop integrated index which indicate source areas for flooding by combining the standard precipitation index (SPI) and the topographic wetness index (TWI);
- To evaluate if a relation can be established between flood prone area(s) and the wetness distribution (soil moisture) in the basin.

1.3.3. Research questions

- How accurate can LISFLOOD simulate stream flow of the upper and middle Awash River Basin?
- Can LISFLOOD be used for identifying flood prone areas?
- Could the combination of TWI and SPI be used for identifying potential areas for flood early warning?
- Can *in-situ* soil moisture observations be used for validating the soil moisture product from ASCAT?

- Could observed soil moisture (ASCAT) be used for identifying areas that serve as an indicator for flood early warning?

1.4. Outline of the thesis

This thesis is structured as follows. In Chapter 1, the introduction on effects of flooding in general and flooding in Awash River basin in particular; and the necessity of developing FEWS in Ethiopia are presented. In addition, the research objectives and questions, hypothesis and thesis outline are presented in this chapter. In Chapter 2, flood early warning uses and concept, uses of rainfall runoff models, application of LISFLOOD model and GEONETCast are described. In Chapter 3, description of the study area and field visit is presented. In Chapter 4, the research methods used for addressing the objectives are presented. In Chapter 5, results obtained using the methods are discussed. In Chapter 6 the research conclusions and recommendations are presented.

2. LITERATURE REVIEW

2.1. Flood early warning

Early Warning Systems (EWSs) evolved about 2 to 3 decades ago. The needs for EWS started to arise in 1970s and 1980s when the prolonged droughts and famines in the West African Sahel and in the Horn of Africa occurred. Since its early development, EWS started to be used for other hazard (technological, hydrological, meteorological, and etc.) for societal risk and vulnerability reduction and toward sustainable development (ESIG-ALERT, 2004). According to United Nations International Strategy for Disaster Redaction (UNISDR) (2009), an EWS is defined as:

“The set of capacities needed to generate and disseminate timely and meaningful warning information to enable individuals, communities and organizations threatened by a hazard to prepare and to act appropriately and in sufficient time to reduce the possibility of harm or loss.”

As the name indicates, Flood EWS is a system by which flood induced hazards can be minimized and prevented. Currently different organizations (Institutes) are working on flood forecasting and early warning at national, continental and global scale (see Table 2-2). For instance, in Africa web-based information systems available that serve for on-going transnational flood forecasting and early warning are limited in number (see Table 2-1). Those initiatives are listed in Table 2-1 below.

Table 2-1: Flood forecasting and early warning initiatives in Africa (After Thieming et al., 2011)

Initiatives	Organizations/Institutes/Country
Flood forecasting initiative	WMO
Associated Program on Flood Management	WMO and GWP
Flood Risk and Response Management Information System	FAO-SWALIM
Early Warning and Humanitarian Emergency Information Center	Republic of Sudan
SERVIR-Africa	NASA, RCMRD & CATHALAC
African Early Warning and Advisory Climate Services in Africa	ACMAD
Global Flood Alert System	Japanese Infrastructure Development Institute
Early Warning System for Flood Events	ITHACA

Specifically in Ethiopia the institute dealing with flood management and flood forecasting and early warning using hydrological modelling are Addis Ababa University (AAU) and National Meteorology Agency (NMA) of Ethiopia (Thieming et al., 2011). However, detailed information on the early warning system in Ethiopia is limited, because one can hardly find scientific research dealing with the issue of flood early warning system in the country. Most of the work done about flood in the country focused on strengthening rescue and relief arrangements during and after major flood disasters.

Table 2-2: Some of the global and continental flood monitoring and early warning systems (This work)

Name	Geographic coverage	Output	Source/link
Dartmouth Flood Observatory	Globe	Map of current floods	http://www.dartmouth.edu/~floods/
IFnet (International Flood Network)	Globe	Precipitation amount maps and flood reports	http://www.internationalfloodnet.org/01_about.html
EFAS, European Flood Alert System	Europe	Daily soil moisture and forecast soil moisture maps for Europe	http://floods.jrc.ec.europa.eu/
NOAA (National Oceanic and Atmospheric Administration's)	US	Maps of current floods River's level measurements from river gauges	http://water.weather.gov/ahps/ http://afws.erh.noaa.gov/afws/index.php?gtype=precip&wfo=gsp

The European flood alert system (EFAS) is a good example of flood EWS, which could be exercised in other parts of the world. EFAS is one of the initiatives working on flood early warning system, which is developed to provide information on possible flooding of river(s) in the European catchments. The main idea in EFAS is to produce probabilistic flood alerts of lead times from 3 to 10 days using different deterministic and ensemble weather forecasts and a hydrological model called LISFLOOD (Thielen et al., 2009). EFAS methodology has also been applied for Juba–Shabelle river basin (adjacent to the Awash River basin) to develop a flood early warning system using different meteorological dataset produced by using probabilistic weather forecasts and a hydrological model (LISFLOOD). More than 85% of the flood events has been successfully detected (Thiemig et al., 2010).

In a flood early warning system the most important input is real-time hydro-meteorological observations provided by weather radar, satellites and/or automatic hydro-meteorological station network (Billa et al., 2006; Budhakooncharoen, 2004). This real-time data can be used in various ways to evaluate flood risks and issues of flood warning. Apart from real time data, probabilistic weather forecasts (Numerical Weather Prediction-NWP) are also playing an important role in providing input for hydrological models to generate warnings scenarios (Burger et al., 2009; Thielen et al., 2009; Thiemig et al., 2010) . Besides having forecasts of the most important input (precipitation), a model needs to be selected that characterizes and simulates the catchment responses for flood early warning.

2.2. Rainfall runoff model selection

Rainfall runoff models are simplified and conceptualized representation of the real world that serve as a tool to transform the meteorological forcing (rainfall and evapotranspiration) into the hydrological response of a catchment (runoff). There are different reasons for using models; but, the main reason is the difficulty to represent the dynamics of hydrological process, which vary in space and time. Beven (2003) states that limited range of measurement techniques and a limited range of measurements in space and time and the need to model the future characteristics of the hydrological processes necessitates using models.

Many kinds of physical, conceptual and empirical (lumped, semi-distributed and distributed) hydrological models are available to study the hydrological processes. Selecting an appropriate model to study a catchment response in terms of stream flow and possibly floods (runoff, simulating a flood) needs an in-depth understanding of the model since each model has its own limitations and advantages. Although, there are no clear rules for making a choice between models, some of the following simple guidelines can

be used. This includes: the problem and/or questions to be answered, the information needed, the hydrologic processes that need to be modelled and the availability of input data for the modelling (Anderson and Burt, 1985). The author tried to select the most suitable model for this study from the SWAT, HEC-HMS and LISFLOOD models based on their successful application for different catchments in different parts of the world and the hydrological processes the models aim to represent. For this study LISFLOOD was selected to evaluate if a flood EWS for the upper and middle Awash River basin could be developed. The LISFLOOD model is described in section 2.3 and a short description of SWAT and HEC-HMS is added below.

The Soil and Water Assessment Tool (SWAT) is a conceptual (semi-distributed) river basin model developed for assessing the impact of land management practice and non-point source pollution in large, complex watersheds (Neitsch et al., 2002). It needs many input data, which is difficult to use in data scarce places like Ethiopia. Moreover, SWAT is more suitable for watershed management practice than for flood modelling, since it is developed for simulating water balance, sediment and nutrient transport (Arnold and Fohrer, 2005).

The Hydrologic Engineering Center's Hydrologic Modelling System (HEC-HMS) developed by the US Army Corps of Engineers, is designed to simulate the rainfall-runoff processes of dendritic watershed systems (Scharffenberg et al., 2006). HEC-HMS is a deterministic model where the parameters values are remain constant for every simulation. In the program, it has been assumed that processes (evaporation, Infiltration) are not coupled, whereas in the real world the amount of infiltration is governed by the moisture content of the soil, which in turn is related to the amount of water removed by evaporation (Scharffenberg et al., 2008).

2.3. LISFLOOD model

2.3.1. Introduction

The short description about the model in this section is modified after for Van Der Knijff and De Roo (2008). For detailed description about the processes, equations and assumptions reference is made to the Revised User Manual (http://floods.jrc.ec.europa.eu/files/lisflood/ec_jrc_lisfloodUserManual_JvdK-AdR.pdf).

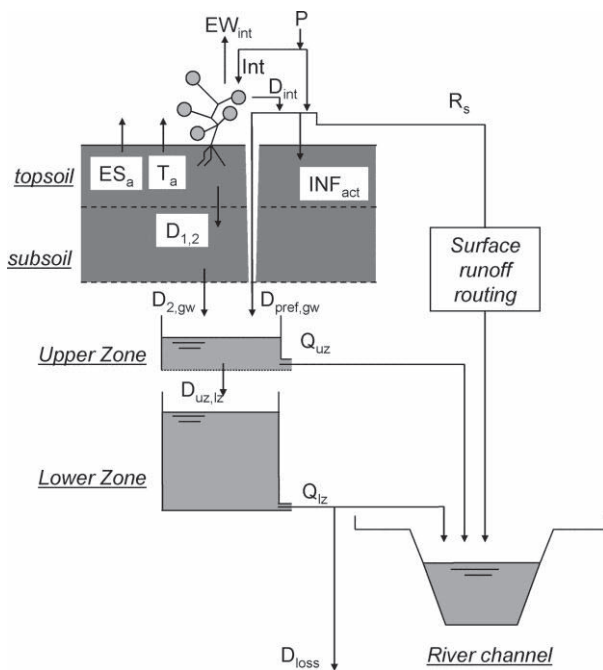
LISFLOOD is a GIS and physically based and spatially distributed hydrological rainfall runoff model, which is developed by the Joint Research Centre (JRC) of the European Commission for simulating hydrological process that occur in catchments (De Roo et.al., 2000). The objective of developing the model was to produce a tool that is capable to be used for large river basin flood forecasting and assessing the effects of river regulation measures, land use and climate change. LISFLOOD has been used with a grid scale of 100 meters for medium size catchment and up to 5000 meters for modelling of different catchments in Europe. The long term water balance and individual flood events can be simulated using daily time step and hourly time intervals respectively. Besides the primary output produced from the water balance run (discharge), the user can define options for all internal rates and state variables (e.g. soil moisture) to be produced as output. Since, the user is privileged by controlling the setup of the model, different output of user-defined points or area can be written as grids or time series.

One of the advantages of using the LISFLOOD model is that, it is implemented in the PCRaster Environmental Modelling language wrapped in a Python based interface, which allows the construction of iterative spatio-temporal environmental models and enables the user to control the model inputs/outputs and the selection of the model modules (e.g. water level, lake and reservoir simulation). Hydrological processes in LISFLOOD are snowmelt, infiltration, interception of rainfall, leaf drainage, evaporation and

water uptake by vegetation, surface runoff, preferential flow (bypass of soil layer), exchange of soil moisture between the two soil layers and drainage to the groundwater, sub-surface and groundwater flow, and flow through river channels (see Figure 2-1).

LISFLOOD is driven by meteorological variables: precipitation intensity, P (mmday^{-1}), potential (reference) evapotranspiration rate of a closed canopy, ET_0 (mmday^{-1}), potential evaporation rate from a bare soil surface, ES_0 (mmday^{-1}), potential evaporation rate from an open water surface, EW_0 (mmday^{-1}), and average 24-hour temperature, T_{avg} ($^{\circ}\text{C}$). The model is constructed in such a way that to solve hydrological process by representing a catchment in to five different components. The components are listed as follows:

- a 2-layer soil water balance sub-model
- sub-models for the simulation of groundwater and subsurface flow (using two parallel interconnected linear reservoirs)
- a sub-model for the routing of surface runoff to the nearest river channel
- a sub-model for the routing of channel flow



Where:

P = precipitation; Int = interception;
 EW_{int} = evaporation of intercepted water;
 D_{int} = leaf drainage;
 ES_a = evaporation from soil surface;
 T_a = transpiration; INF_{act} = infiltration;
 R_s = surface runoff;
 $D_{1,2}$ = drainage from top to subsoil;
 $D_{2,gw}$ = drainage from subsoil to upper groundwater zone;
 $D_{pref,gw}$ = preferential flow to upper groundwater zone;
 $D_{uz,lz}$ = drainage from upper to lower groundwater zone;
 Q_{uz} = outflow from upper groundwater zone;
 Q_{lz} = outflow from lower groundwater zone;
 D_{loss} = loss from lower groundwater zone.

Figure 2-1: Schematic representation of LISFLOOD model without including snowmelt (Source: Van Der Knijff et al., 2008)

2.3.2. Previous studies

A number of scholars have applied LISFLOOD model for different types of applications and to assess the model performance. It has been applied mostly in European catchments and in the Horn of Africa in Somalia's Juba-Shabelle basin for the purpose of flood forecasting and to develop flood early warning system (De Roo et al., 2000; Thiemiig et al., 2010). To mention some studies: Feyen et al. (2007) have performed automated calibration using daily discharge observations from the Meuse catchment (France, Belgium, Germany and The Netherlands) to assess the model performance by applying the Shuffled Complex Evolution Metropolis (SCEM-UA) global optimization algorithm. According to the calibration results they have found that, SCEM-UA algorithm was able to identify posterior parameter distributions in less than 2500 iterations and using 2 years of measured daily discharges calibration parameters of the

LISFLOOD model were well optimized. De Roo et al., (2003) have developed a distributed catchment model LISFLOOD for the Oder basin (The Czech Republic, Poland and Germany) and the Meuse catchment (France, Belgium, Germany and The Netherlands) to investigate the cause of flooding and the influence of land use, soil characteristics and antecedent catchment moisture conditions. By using the model in case of the Meuse catchment, they have found that due to the land use change (1975 to 1992) flood risk has become slightly larger. Laguardia and Niemeier (2008) compared the LISFLOOD modelled and ERS/SCAT derived soil moisture estimates of the entire European catchments. The result indicates that LISFLOOD modelled and the ERS/SCAT derived soil moisture products match well over large areas in Europe, except the Scandinavia regions. Dankers et al., (2007) used high-resolution climate model (HIRHAM) data to drive the hydrological model LISFLOOD for simulating flood hazards in the upper Danube basin (Europe). In the study, they have found that LISFLOOD has shown good simulation as long as the prediction from the climate model is representative, although the accuracy of the climate model limited the simulation results from LISFLOOD. Salamon and Feyen (2009) have applied sequential data assimilation techniques with the particle filter to assess parameter, precipitation, and predictive uncertainty of LISFLOOD for the Meuse catchment upstream of Borgharen (Maastricht, the Netherlands).

In most of the studies, LISFLOOD has shown good performance. Especially, the promising performance of the model in the tropical zone like Juba-Shabelle river basin has contributed to select the model to for flood EWS in the Awash River Basin.

2.4. GEONETCast

GEONETCast is a global network of satellite based data dissemination systems that provide environmental data to a worldwide user community. The current partners within the GEONETCast initiative include the National Oceanic and Atmospheric Administration (NOAA), the World Meteorological Organization (WMO) and EUMETSAT, as well as many third party data providers (see Figure 2-2). GEONETCast is user driven, user friendly and low cost information dissemination service, which aims at providing worldwide information as a basis for sound decision making in a number of essential benefit areas, which include public health, energy, agriculture, weather, water, climate, natural disasters and ecosystems. In-depth explanation about GEONETCast can be found on the GEO website (<http://www.earthobservations.org/geonetcast.shtml>).

To support importing data disseminated through EUMETCast-GEONETCast into the freeware and open source remote sensing and GIS software package, ILWIS, the GEONETCast toolbox is developed. The toolbox is used as plug-in in ILWIS. It provides a set of utilities that facilitate easy import of various satellite and environmental data/products that are disseminated via GEONETCast, into a common GIS environment (see Figure 2-3). Description of the toolbox as well as where to download all the data and how to install and configure it can be found in the installation, configuration and user guide (Maathuis et al., 2011).

Figure 2-2 below shows the GEONETCast system overview and Figure 2-3 shows the GEONETCast toolbox version 1.3 menu as plug-in with in ILWIS software.

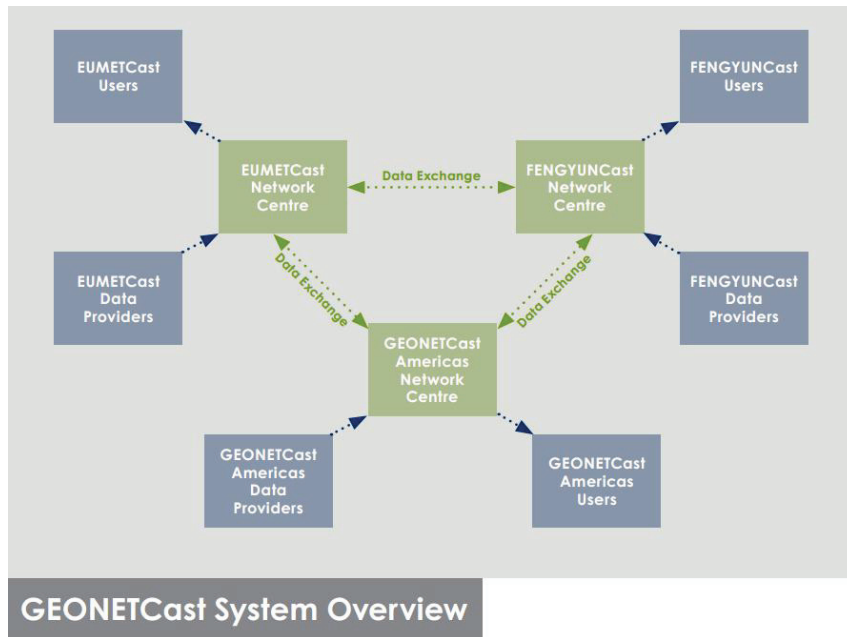


Figure 2-2: GEONETCast system overview (EUMETSAT, October 2007¹)



Figure 2-3: GEONETCast toolbox version 1.3 menu (source: plug-in with in ILWIS software)

¹ http://www.eumetsat.int/groups/cps/documents/document/PDF_BR_E01_EN.pdf

3. STUDY AREA AND DATA SETS

3.1. Study area

The Awash River Basin is the fourth largest catchment in Ethiopia (110,000km²) and the seventh in terms of mean annual runoff (4.6BM³). The total length of the main course is some 1,200km and is the principal stream of an endorheic² drainage basin covering parts of the Oromia, Somali, Amara and Afar region. The geographical location of the basin is between latitudes of 7°25'N and 12°25'N and longitude of 38°13'E and 43°17'E (Taddese et al., 2006). The area considered for this research only covers the upstream and some middle part of the basin, which is about 31483km² (see Figure 3-1 and Figure 3-2).

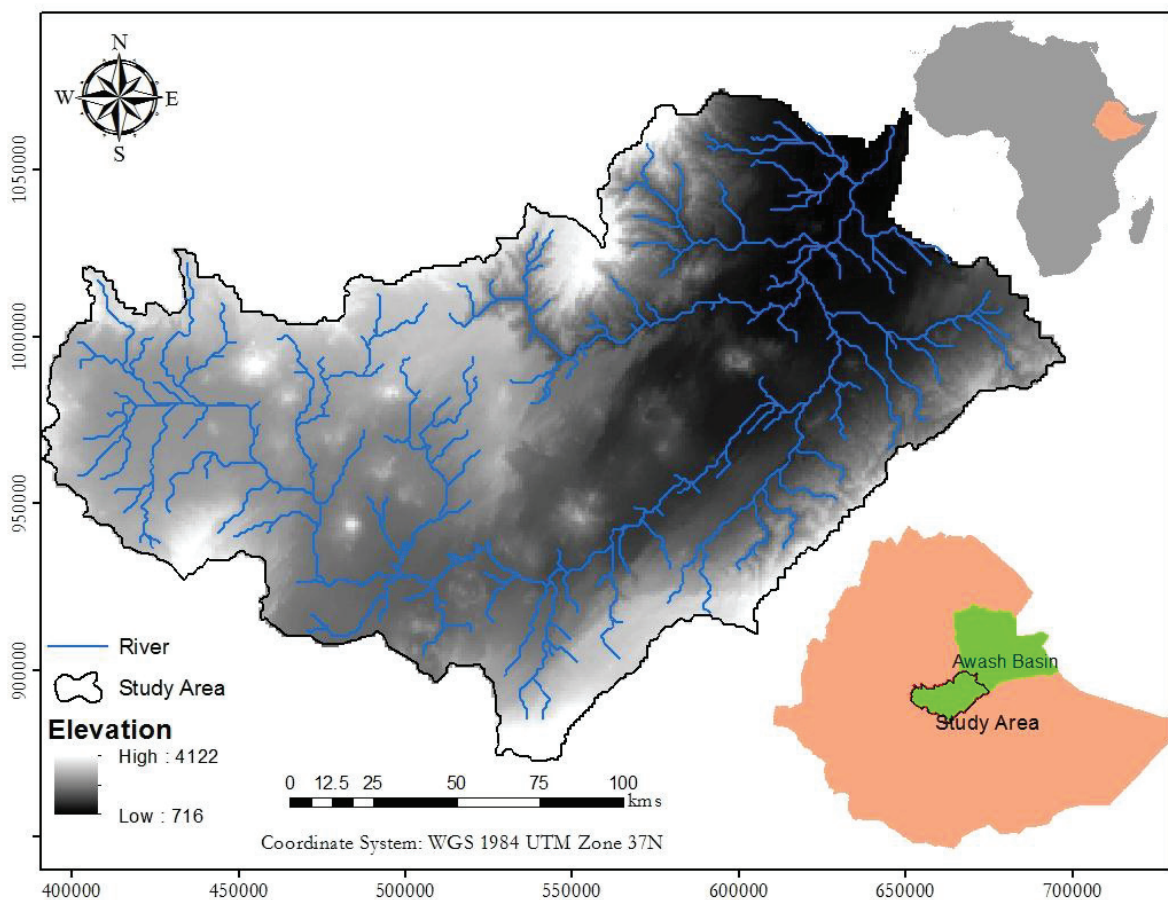


Figure 3-1: Location map of the study area

² Endorheic basin is a closed drainage basin that retains water and allows no outflow to other bodies of water such as rivers or oceans. Normally, water that has accrued in a drainage basin eventually flows out through rivers or streams on Earth's surface or by underground diffusion through permeable rock, ultimately ending up in the oceans. (Source: Wikipedia)

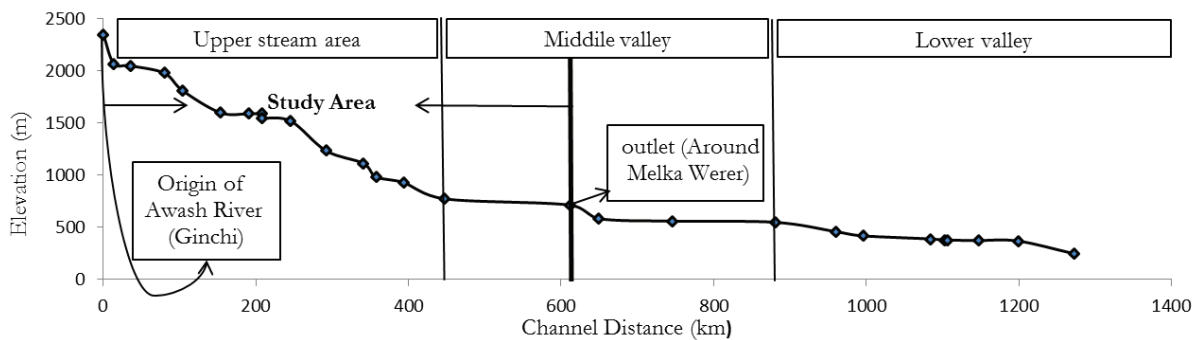


Figure 3-2: Longitudinal Section of Awash River Channel (Source: Halcrow, 2006)

The basin has two main physiographic components; the Ethiopian plateau, and the Rift Valley, which covers most of the basin. The topography of the plateau is generally flat with elevations ranging from 2,000m to 2,500m. The Rift Valley area is seismically active and there is a well-documented history of earthquakes in the basin and there are still places having active volcanic areas (MoWE, 2011).

The climate of the Awash River Basin is affected by the Inter-Tropical Convergence Zone (ITCZ). The seasonal rainfall distribution in the basin results from the annual migration of the ITCZ. Plateaus in the basin (>2,500m.a.s.l) mostly receive 1,400 - 1,800mm of rainfall per year. Whereas, mid-altitude (600 – 2,500m.a.s.l) and lowlands regions (<600m.a.s.l) receive rainfall of 1,000 - 1,400mm and less than 200mm per year respectively. The rainfall distribution in the highland areas is bimodal, with a short rainy season during March and April and the long rainy season from June to September. The mean annual temperatures range from 20.8°C to 29°C and the annual average wind speed is 1.2ms⁻¹ (MoWE, 2011).

The soil types found in the study area, according to FAO classification (1998), are Pellic Vertisol, Vertic Cambisol, Chromic Luvisols, Luvic Phaeozems, and Lithosols. However, the dominant soil types are Cambisols and Vertisols. Vegetation cover in the upper and middle parts of the basin is grassland with some scrubland and riparian forest along the Awash River. Some of the plant species include *Balanites aegypticus*, *Salix subserata*, *Flueggia virosa*, *Carissa edulis*, *Rumex nervosus*, *Tamarindus indica*, *Ulcea schimperii* and *Acacia* species (Halcrow, 2006).

Awash River has major economic value for the country. In the study area there are two sugarcane factories ('Wanji-Shoa': located 15km to the south of Adama city and 'Matahara': located 10km southeast of Matahara town), which are contributing in the nation's development. Besides these, there are many large and small-scale irrigation projects ('Tendaho', 'Kesem', 'Awash Agro-Industry', etc.) implemented in the basin, which have also a great development contribution. Due to its strategic location, as well as the availability of land and water resources, the Awash Valley is the most developed area in Ethiopia with respect to irrigated agriculture. In the upper valley part of the basin, sugar cane is the dominant crop produced and used by the Wonji-Shoa and Matahara sugar factories. In addition to sugar cane; citrus fruits, vegetables (mainly tomatoes), maize, groundnut, and cotton are grown in the upper valley. In the lower valley, cotton is also the dominant crop with over 90% of the irrigated area on large farm enterprises (Taddese et al., 2006).

3.2. Data Sets

For this research, remote sensing data and ground-based measurements were used. Most of the remote sensing data were obtained from GEONETCast and FEWS NET data streams and the *in-situ* data were collected during field visit in Ethiopia for two weeks. As part of the field visit Awash Basin Authority

(ABA), Ministry of Energy and Water (MoEW), National Meteorological Agency (NMA) and Water Works Design and Supervision Enterprise (WWDSE) offices were visited to collect secondary data and information on previous works done on flooding of Awash River Basin. Besides, the collection of secondary data, a visit to the flood prone areas and on flood occurrence experts and local peoples were contacted. Also field campaign was undertaken to measure surface soil moisture (5 – 10cm) at varies sites by use of Theta Probe.

3.2.1. Data from offices

Meteorological data (rainfall, humidity, sunshine hour, maximum and minimum temperature) from NMA and discharge data (stream flow) from MoEW for various stations (see Figure 3-3 and Table 3-1) in the basin were collected. Also, a digital soil type map (according to FAO 1998 classification) and digital land cover map (produced from MODIS image) from Awash Basin Authority (ABA) were obtained. Detailed description on the type of data and maps collected are presented below.

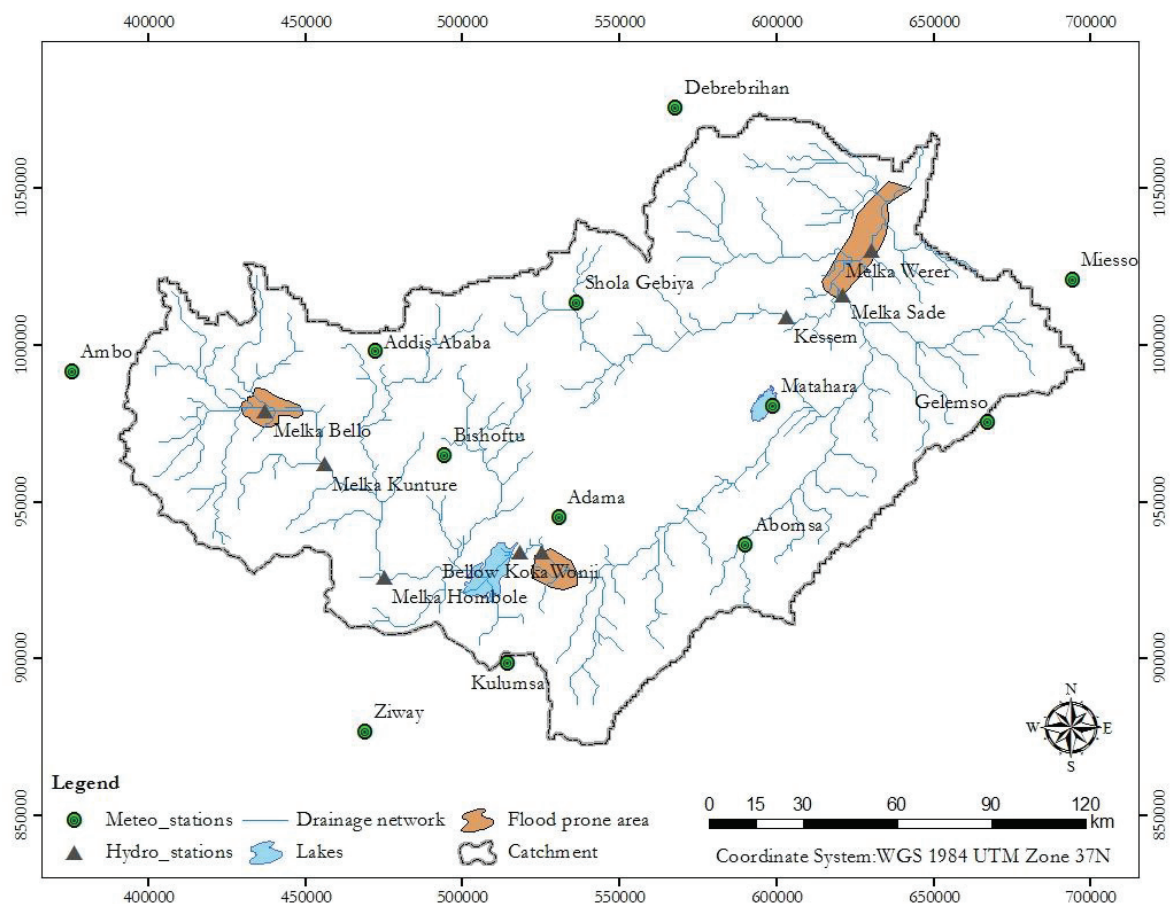


Figure 3-3: Meteorological and Hydrological stations in the study area

Observed stream flow data from 22 hydrological stations (river gauges) that are located in the main reach and tributaries were obtained from MoEW and 12 meteorological stations that have the meteorological variables (maximum and minimum temperature, humidity, wind speed, sunshine hour and rainfall) were obtained from NMA. Time series of the observed stream flow data are not always complete and reliable as shown in Figure 3-4. Figure 3-4 shows the observed stream flow hydrograph of selected 6 stations. In Table 3-1, the name and the corresponding period of record of the stations are presented.

Table 3-1: Meteorological and Hydrological stations in the study area

Meteorological Stations			
Station Name	Period of Record	Station Name	Period of Record
ADDIS ABABA	2006-2010	GELEMSO	2006-2010
ABOMSA	2006-2010	KULUMSA	2006-2010
AMBO	2006-2010	MATAHARA	2006-2010
ADAMA	2006-2010	MIESSO	2006-2010
BISHOFTU	2006-2010	SHOLA GEBIYA	2006-2010
DEBREBRIHAN	2006-2010	ZIWAY	2006-2010

Hydrological Stations									
Station Name	MELKA BELLOO	MELKA KUNTURE	MELKA HOMBOLE	BELLOW KOKA	WONJI	MELKA SADE	KESSEM	MELKA WERER	
Period of Record	1987 2010	1980 2008	1980 2009	1980 2009	1980 2009	1983 june2009	1980 2008	19802 009	
Hydrological Variable(s)	Stream flow (Discharge [m^3s^{-1}])								

Selecting suitable gauge(s) having continuous records for model calibration and validation was challenging, because of the gaps in the observed stream flow data. In order to check the reliability of the data double mass curve analysis was applied. The results of double mass curve analysis are presented in Chapter 5 (section 5.3).

Observed Stream Flow Hydrographs

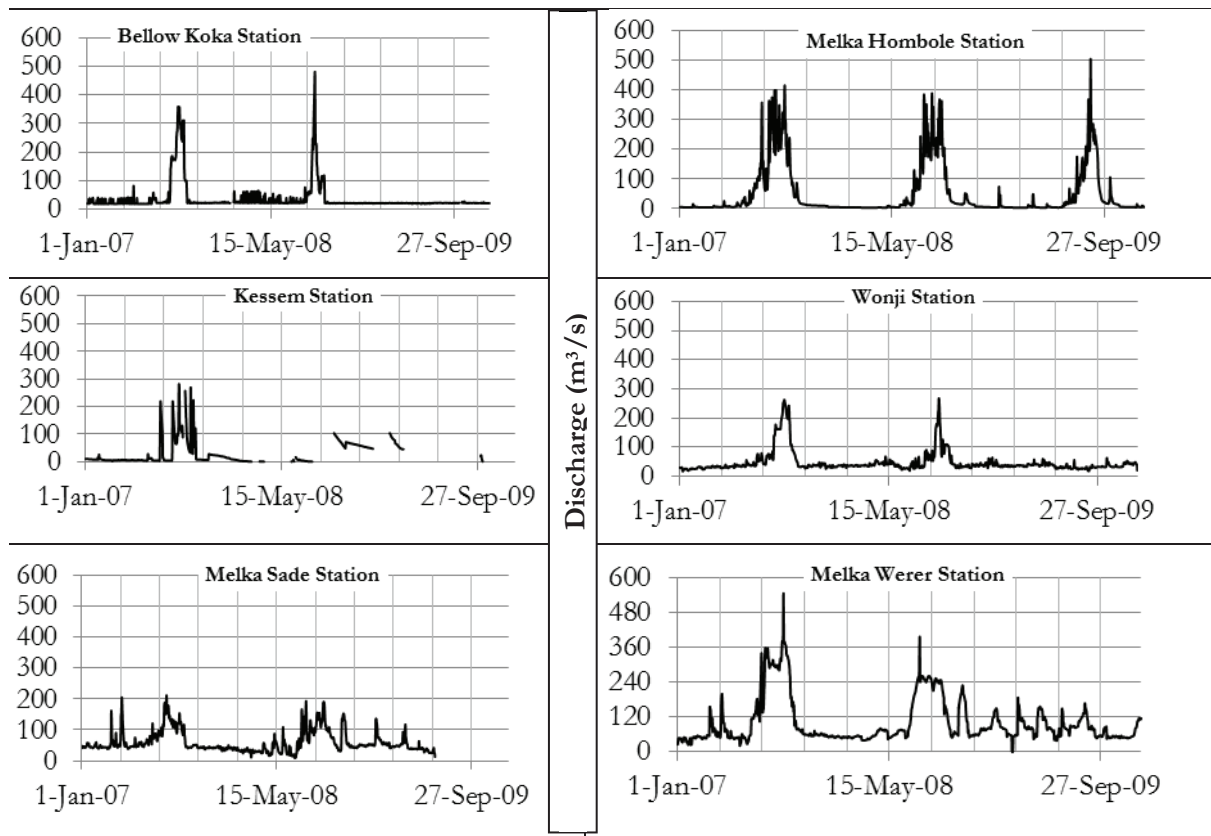


Figure 3-4: Observed stream flow hydrograph of selected 6 stations

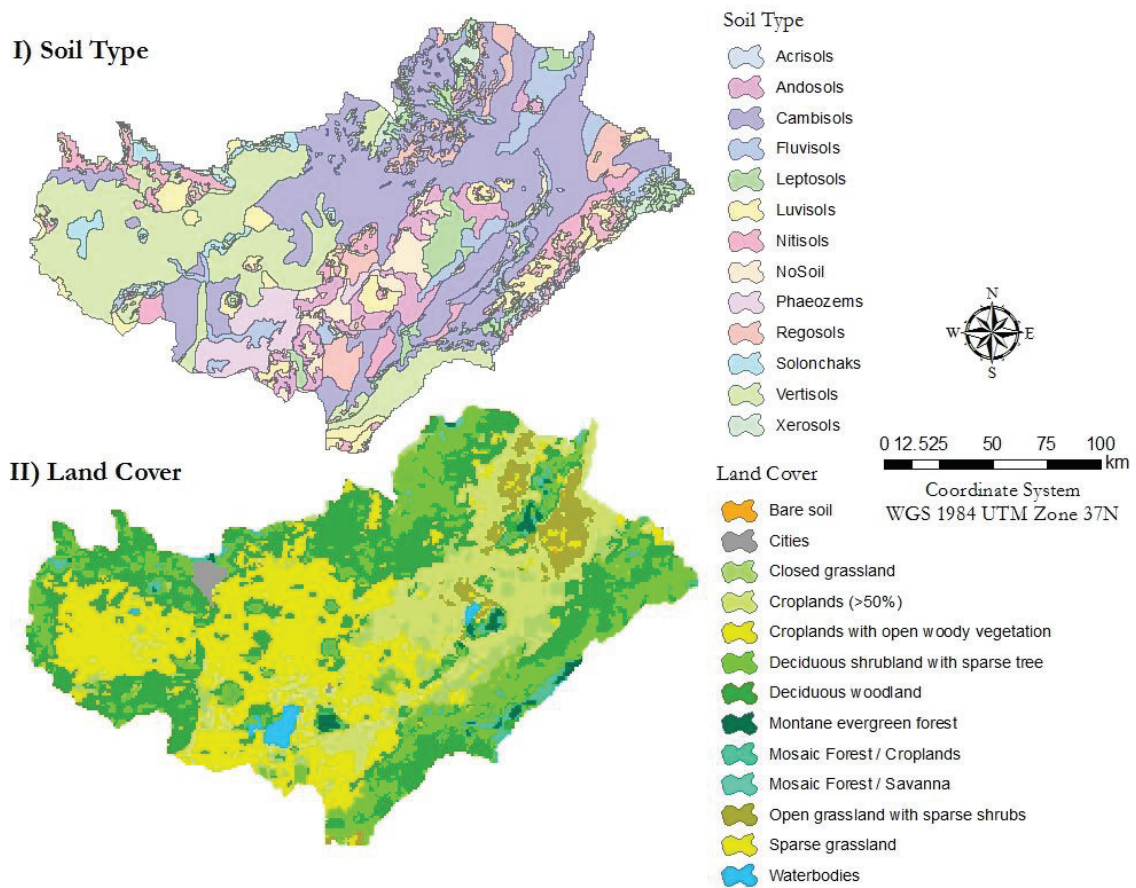


Figure 3-5: Soil type and land cover of the study area (source: Awash Basin Authority, after Halcrow, 2006)

3.2.2. Satellite data products

Remote sensing products used for this study were Global CMORPH (precipitation), Satellite Application Facility-LAI (leaf area index), FEWS NET Global Potential Evapotranspiration (PET), ASCAT (surface soil moisture) and SRTM-DEM (elevation). Except SRTM-DEM all the products can be downloaded using GEONETCast toolbox plug-in under ILWIS. The temporal and spatial resolution and source of the data sets are presented in Table 3-2. Detailed product descriptions and the processing steps are presented in Chapter 4 (section 4.2.).

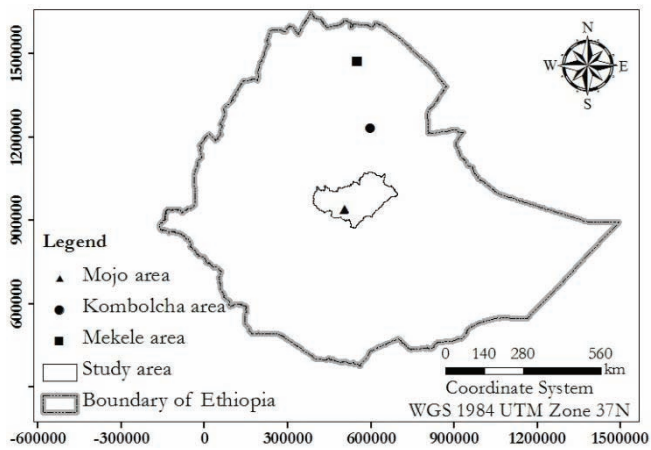
Table 3-2: Satellite products with their spatial and temporal resolutions, source and period of records

Global CMORPH	Spatial resolution	0.25 ^o by 0.25 ^o
	Temporal resolution	3hrs (accumulated to daily)
	Period of record	2002 up to 2011
	Source (URL)	ftp://ftp.cpc.ncep.noaa.gov/precip/global_CMORPH/3-hourly_025deg
SAF Leaf Area Index (LAI)	Spatial resolution	3km
	Temporal resolution	Daily
	Period of record	2007 up to 2010
	Source (URL)	http://landsaf.meteo.pt

FEWS NET Global Potential Evapotranspiration (PET)	Spatial resolution	1° by 1°
	Temporal resolution	Daily
SRTM (DEM)	Period of record	2001 up to 2011
	Source (URL)	http://edcftp.cr.usgs.gov/pub/data/fewsips/global/
Surface soil moisture (ASCAT)	Spatial Resolution	1km
	Source (URL)	http://srtm.csi.cgiar.org/SELECTION/inputCoord.asp
Surface soil moisture (ASCAT)	Spatial resolution	12.5km
	Temporal resolution	Twice a day (ascending and descending orbit)
	Period of record	2006 up to 2011

3.2.3. In-situ measured data

In-situ surface soil moisture (5-10cm depth) measurement using a theta probe was done. The samples were taken based on accessibility of the site and representative area and time to validate the ASCAT surface soil moisture. The samples were taken on different land cover types for two dates, September 16 and 21 2011 and three locations in Ethiopia (Mojo, Kombolcha and Mekele areas). Sites are indicated and shown in Figure 3-6.



a)



Figure 3-6: Sample sites for surface soil moisture measurement and photographs taken during field visit

4. RESEARCH METHOD

4.1. Introduction

In this chapter data processing and the method applied in this research are presented. The research has three phases. In the first phase a rainfall runoff model for the study area is developed. It includes input data preparation, model setup, model initialization, sensitivity analysis of the model input parameters, model calibration, model validation and stream flow and water level simulation. The second phase is validation of ASCAT surface soil moisture (ASCAT-SSM) product using *in-situ* data, standard precipitation index (SPI) computation and Topographic Wetness Index (TWI) processing. The third phase aims to develop a relation between ASCAT- surface soil moisture and/or SPI with the stream flow hydrograph and/or water level in the river channel. The conceptual flow chart, which shows the overall research process, is presented in Figure 4-1 below.

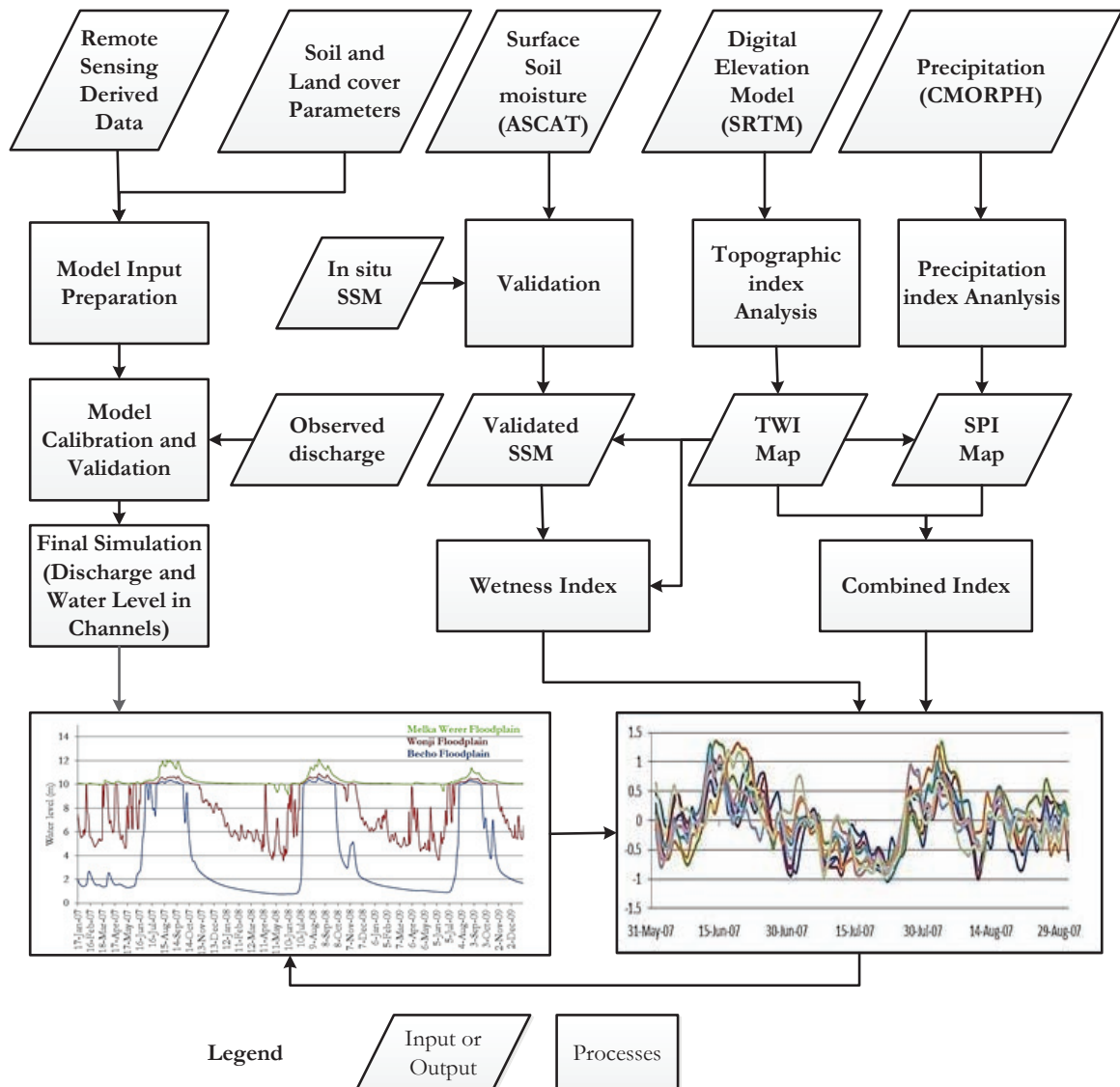


Figure 4-1: Flow chart of the research method

4.2. Data preprocessing

Input data sets for the model are characterized by specific spatial and temporal resolution, format and coordinate system. LISFLOOD model is designed to be applied across a wide range of spatial and temporal scales; and it has been applied so far for a spatial resolution of 100m for medium-sized catchments and up to 5000m for whole of Europe (De Roo et al., 2000). In this study to model the rainfall runoff relation of the study area (31,483km²), spatial resolution 1km x 1km and temporal resolution of daily time step were selected.

The input data used for the model have different coordinate systems, spatial and temporal resolution. So, in order to meet the objective of the study and for further analysis, the input data sets were processed to a common spatial (1km x 1km) and temporal (daily) resolution and a WGS 1984 UTM Zone 37N coordinate system was adopted. For pre-processing various techniques were used as introduced in the following sections.

4.2.1. Rainfall data

For any hydrologic model rainfall is an important input as it serves as a model forcing term. Rainfall can be from ground-based (radar and/or rain gauges) measurement or from satellite estimates. Even though ground-based measurements are considered to provide the most accurate value, the spatial coverage of such measurements often is very poor in many regions of the world and access to data from those measuring gauges are very limited. Currently a number of satellite rainfall products are available. For this study the Climate Prediction Centre CMORPH and EUMETSAT's Multi-sensor Precipitation Estimates (MPE) are selected.

CMORPH precipitation estimates have been derived from low orbiting satellite microwave observations and geostationary satellite infrared (IR) data. The IR data from the meteorological satellites are used as a means to transport the microwave derived precipitation features during periods when microwave data are not available (Joyce et al., 2004). The passive microwaves used are from:

- Special Sensor Microwave/Imager (SSM/I) on-board of the United States Defence Meteorological Satellite Program (DMSP) 13, 14 and 15;
- Advanced Microwave Sounding Unit-B (AMSU-B) of National Oceanic and Atmospheric Administration (NOAA) 15, 16, 17 and 18;
- Advanced Microwave Scanning Radiometer (AMSR-E) on-board of NASA's Aqua satellite; and
- TRMM Microwave Imager (TMI) on-board of NASA's Tropical Rainfall Measuring Mission (TRMM) spacecraft.

The MPE rainfall estimate is derived from microwave measurements of the Special Sensor Microwave/Imager (SSM/I) on-board of the US-DMSP satellites and brightness temperature from the IR channel (10.8) of the Meteosat Second Generation (MSG) satellites (EUMETSAT, 2011).

After comparing the satellite rainfall data (CMORPH and MPE) with the ground based rainfall measurements, the CPC-CMORPH rainfall data was used for daily simulations in the LISFLOOD model. The CMORPH data is compressed using the standard UNIX compress function (files having a suffix of '.Z') and composed of two types of rainfall data. These are the microwave and CMORPH precipitation estimates. The CMORPH precipitation product (temporal resolution 3-hours) was downloaded and imported using GEONETCast toolbox utility in ILWIS. To download and import the data, a batch file has been developed in the GEONETCast toolbox, which produces rainfall maps in an ILWIS raster format.

The ILWIS raster format rainfall map was resampled to 1km x 1km spatial resolution, and to the WGS-1984 UTM Zone 37N coordinate system. Then, the 3 hourly rainfall maps were accumulated to produce maps daily rainfall. Finally, the daily rainfall ILWIS raster format was exported to PCRaster format by using the export functionality in ILWIS, since PCRaster is the format that LISFLOOD uses. A script has been created to automate the resampling and exporting process of the data set for the whole study period (2007 – 2009). Figure 4-2 shows the command line syntax of the script used to convert CMORPH rainfall ILWIS raster to PCRaster format.

```

ID:\ilwis372\gdal_translate.exe -of PCRaster D:\Rainfall_preprocess\CMORPH\cmorph_awash20070101.mpr D:\Rainfall_preprocess\CMORPH\PCRaster\pr000000.001
ID:\ilwis372\gdal_translate.exe -of PCRaster D:\Rainfall_preprocess\CMORPH\cmorph_awash20070102.mpr D:\Rainfall_preprocess\CMORPH\PCRaster\pr000000.002
ID:\ilwis372\gdal_translate.exe -of PCRaster D:\Rainfall_preprocess\CMORPH\cmorph_awash20070103.mpr D:\Rainfall_preprocess\CMORPH\PCRaster\pr000000.003
ID:\ilwis372\gdal_translate.exe -of PCRaster D:\Rainfall_preprocess\CMORPH\cmorph_awash20070104.mpr D:\Rainfall_preprocess\CMORPH\PCRaster\pr000000.004
ID:\ilwis372\gdal_translate.exe -of PCRaster D:\Rainfall_preprocess\CMORPH\cmorph_awash20070105.mpr D:\Rainfall_preprocess\CMORPH\PCRaster\pr000000.005
ID:\ilwis372\gdal_translate.exe -of PCRaster D:\Rainfall_preprocess\CMORPH\cmorph_awash20070106.mpr D:\Rainfall_preprocess\CMORPH\PCRaster\pr000000.006
ID:\ilwis372\gdal_translate.exe -of PCRaster D:\Rainfall_preprocess\CMORPH\cmorph_awash20070107.mpr D:\Rainfall_preprocess\CMORPH\PCRaster\pr000000.007
ID:\ilwis372\gdal_translate.exe -of PCRaster D:\Rainfall_preprocess\CMORPH\cmorph_awash20070108.mpr D:\Rainfall_preprocess\CMORPH\PCRaster\pr000000.008
ID:\ilwis372\gdal_translate.exe -of PCRaster D:\Rainfall_preprocess\CMORPH\cmorph_awash20070109.mpr D:\Rainfall_preprocess\CMORPH\PCRaster\pr000000.009
ID:\ilwis372\gdal_translate.exe -of PCRaster D:\Rainfall_preprocess\CMORPH\cmorph_awash20070110.mpr D:\Rainfall_preprocess\CMORPH\PCRaster\pr000000.010
ID:\ilwis372\gdal_translate.exe -of PCRaster D:\Rainfall_preprocess\CMORPH\cmorph_awash20070111.mpr D:\Rainfall_preprocess\CMORPH\PCRaster\pr000000.011
ID:\ilwis372\gdal_translate.exe -of PCRaster D:\Rainfall_preprocess\CMORPH\cmorph_awash20070112.mpr D:\Rainfall_preprocess\CMORPH\PCRaster\pr000000.012
    
```

Figure 4-2: Command line syntax of the script used to convert CMORPH rainfall ILWIS raster format to PCRaster time series maps of rainfall

4.2.2. Potential Evapotranspiration

Potential evapotranspiration (PET) is one of the meteorological forcing terms used in LISFLOOD model. In LISFLOOD approach evapotranspiration is explained as reference evapotranspiration of a closed canopy (ET_o : mmday^{-1}), as potential evaporation of bare soil surface (ES_0 : mmday^{-1}) and as potential evaporation of open water surface (EW_0 : mmday^{-1}) are used as forcing parameters in LISFLOOD (Van Der Knijff et al., 2008).

4.2.2.1. Reference evapotranspiration (ET_o)

Reference evapotranspiration is defined as “the rate of evapotranspiration from a hypothetical reference crop with an assumed crop height of 0.12m, a fixed surface resistance of 70sm^{-1} and an albedo of 0.23, closely resembling the evapotranspiration from an extensive surface of green grass of uniform height, actively growing, well-watered, and completely shading the ground” by Allen et al., 1998 after Penman (1948).

$$ET_o = \frac{0.408\Delta(R_n - G) + \gamma \frac{900}{T + 273} u_2 (e_s - e_a)}{\Delta + \gamma(1 + 0.34u_2)} \quad (4.1)$$

Where; ET_o is reference evapotranspiration [mmday^{-1}], R_n is net radiation at the crop surface [$\text{MJm}^{-2}\text{day}^{-1}$], G is soil heat flux density [$\text{MJm}^{-2}\text{day}^{-1}$], T is air temperature at 2m height [$^{\circ}\text{C}$], u_2 is wind speed at 2m height [ms^{-1}], e_s is saturation vapour pressure [kPa], e_a is actual vapour pressure [kPa], $e_s - e_a$ is saturation vapour pressure deficit [kPa], Δ is slope of vapour pressure curve [$\text{kPa}^{\circ}\text{C}^{-1}$], γ is psychrometric constant [$\text{kPa}^{\circ}\text{C}^{-1}$] (Allen et al., 1998).

The reference evapotranspiration used in this study are ETo based on *in-situ* data and Global ETo from Famine Early Warning System Network (FEWS NET, 2011). The *in-situ* based ETo was computed using meteorological parameters (temperature, sunshine hours, wind speed and humidity) collected from the 12 stations during the field visit. The stations meteorological parameters used for ETo computation have missing values. To fill the missing values a simple averaging technique was used, whereby the missing value is set equal to an average of the same day for years observations are available (2006 – 2010). Following the gap filling, the ETo estimates for each station were calculated using the FAO Penman-Monteith method (Equation 4.1). The *in-situ* based ETo was interpolated so to yield an ETo map for the study area.

To interpolate the ETo values, a weighted inverse distance interpolation technique was used. For interpolation, it is necessary to select an appropriate weight power (how nearest points to be weighted), number of stations to be considered, distance and spatial resolution used determines the accuracy of the interpolated value. In order to test the accuracy of the interpolation method and to select the possible weight power for interpolation, the interpolated ETo value using all the stations was cross validated with interpolated ETo values using two independent stations (see result section 5.1).

On the other hand, daily global potential evapotranspiration (PET) product disseminated by FEWS NET was used as meteorological forcing term in LISFLOOD model. FEWS NET PET is calculated using meteorological parameters (air temperature, atmospheric pressure, wind speed, relative humidity, and solar radiation) generated every 6 hours by the National Oceanic and Atmospheric Administration (NOAA) using the Global Data Assimilation System (GDAS). The FEWS NET ETo is computed in a spatially distributed fashion using the Penman-Monteith equation for each 6-hour period and then summed to obtain daily value (FEWS NET, 2007).

FEWS NET ETo product is in a gridded (.bil) file format. By using a batch routine provided in the GEONETCast toolbox the FEWS NET ETo for the period 2006 - 2010 were downloaded and imported for the analysis. After importing, using a script in ILWIS (to automate the processing) the data were resampled as described above. Finally, ETo maps in ILWIS raster format was exported to PCRaster format using the export functionality in ILWIS and used as input in the model.

4.2.2.2. Potential evaporation from open water (EW0)

Potential open water evaporation is one of the inputs in LISFLOOD. In this study, EW0 was computed from the reference evapotranspiration (FEWS NET and *in-situ* based ETo) using the concept of pan evaporation, whereby the open water evaporation is considered to be pan evaporation. Pan evaporation is related to the reference evapotranspiration by an empirically derived pan coefficient (Maidment, 1992). So, in order to obtain the open water evaporation equation 4.2 is used.

$$ET_{pan} = ET_o / K_{pan} \quad (4.2)$$

Where; ETo is reference evapotranspiration [mmday⁻¹], Kpan is pan coefficient [-], Epan is pan (open water) evaporation [mmday⁻¹].

Selection of the pan coefficient depends on relative humidity, wind speed and the surrounding land cover of the study area. A Kpan value of '0.75' is normally selected in case a pan is surrounded by short green grass, mean relative humidity is between 40 - 70% and wind speed is less than 2 ms⁻¹ (Allen et al., 1998). These characteristics applies to the study area (average wind speed of 1.38 ms⁻¹ and mean relative humidity in the range of 40 - 70% (see section 3.1)). A PCRaster map of a Kpan having value of 0.75 was created using the 'mapattr' functionality in the PCRaster. Consequently, potential open water evaporation

PCRaster maps were obtained dividing the potential evapotranspiration PCRaster maps by ‘0.75’ using the ‘pcrcalc’ function in the PCRaster and to automate the process a batch file has been created to produce the EW0 of the whole study period (see Table 4-1).

Table 4-1: The form of batch file used to convert ETo to EW0

dr1...\pcrcalc	dr2...\e0000000.001	=	dr3...\et000000.001	div	dr4...\kpan.map
.
.
.
dr1...\pcrcalc	dr2...\e0000000.1097	=	dr3...\et000000.1097	div	dr4...\kpan.map

Where: dr₁ is directory for PCRaster, dr₂ is directory for output directory (open water evaporation), dr₃ is output directory (ETo) and dr₄ is input directory (pan coefficient), div is divide.

4.2.2.3. Potential evaporation from bare soil (ES0)

As one of the input meteorological forcing terms in the LISFLOOD model, in this study, the daily potential evaporation from bare soil is calculated according to the empirical relation between ES0 and ETo (equation 4.3) presented in Food and Agriculture Organization Irrigation and Drainage (FAO-56) handbook by Allen et al., (1998; 2005).

$$ES0 = K_e ETo \tag{4.3}$$

Where; ES0 is the potential rate of evaporation from bare soil [mmday⁻¹], ETo is reference evapotranspiration during the initial period [mmd⁻¹] and K_e is the daily evaporation coefficient. In this study K_e of 1.15 was used (Allen et al., 2005).

PCRaster maps of the potential soil evaporation rate (ES0) were calculated by multiplying the reference evapotranspiration rate (ETo) PCRaster maps by the constant value map of ‘1.15’ using ‘pcrcalc’ and ‘multiplication’ function in PCRaster.

4.2.3. Leaf Area Index

EUMETSAT promotes several Satellite Application Facilities (SAF’s), among them the Land Surface Analysis-SAF is dedicated to the development and operational retrieval of products based on Meteosat Second Generation (MSG) and Meteorological Operational satellite program (MetOp) satellites over continental areas. Leaf area index (LAI) is one of the products estimated from the MSG SEVIRI instrument over Europe, Africa, the Middle East, and parts of South America since January 2007. It can be accessed via the Land Surface Analysis-SAF web page. A detailed description of the processing algorithm and product description can be found on the product user manual available on EUMETSAT website (SAF, 2011).

LAI is an important input for the LISFLOOD model, since it is used as input in several processes such as interception, evaporation of intercepted water, water uptake by plants roots and transpiration, and direct evaporation from the soil surface. Daily LAI (HDF5 format) of the years 2007 - 2009 were downloaded from ‘http://landsaf.meteo.pt/’ website. Next, the LAI is imported into ILWIS raster format using the GEONETCast toolbox functionality. Like the other input parameters (rainfall and evapotranspiration), the ILWIS raster format LAI data is resampled to a spatial resolution of 1km x 1km and WGS-1984 UTM Zone 37N projection. Lastly, the resampled daily LAI ILWIS raster maps were exported to PCRaster using the export functionality in ILWIS.

4.2.4. Land cover and soil type

Several input parameters in the LISFLOOD model such as soil depth, soil texture, saturated soil moisture, saturated hydraulic conductivity, pore size index, fraction of forest, crop coefficient, Manning's coefficient of roughness and direct runoff fraction are derived from the land cover and soil type of the study area. Digital (ArcGIS format) land cover and soil type maps obtained from the Ethiopian Awash Basin Authority (ABA) (see Figure 3-5) were used for this study. The land cover map was produced by Halcrow (2006) from MODIS data (spatial resolution 1000m) and the soil type was produced based on the FAO-1998 classification. The land cover and soil maps have an attribute table, which contains the land cover and soil type's description (see Figure 3-5).

The land cover and soil type maps have been converted to raster maps and reclassified to numeric codes. According to the codes, which represent different land cover classes and soil types; the following maps and tables were derived as suggested by Van Der Knijff and De Roo (2008) as described in the LISFLOOD model user manual.

- Crop coefficient, Manning's roughness, crop group number and rooting depth for each land cover class in a table in '.txt' file format (Van Der Knijff and De Roo 2008);
- PCRaster maps of direct runoff fraction obtained by classifying the land cover and assigning the corresponding values (i.e. fraction urban area for each cell: values range from 0 means no urban area at all and 1 means pixel is 100% urban);
- PCRaster maps of forest area obtained by classifying the land cover and assigning the corresponding values (i.e. forest fraction for each cell: values range from 0 means no forest at all and to 1 means pixel is 100% forest);
- Upper and lower layer saturated and residual volumetric soil moisture content, pore size index and saturated hydraulic conductivity of each soil type in a table in '.txt' file format;
- PCRaster maps of soil texture (upper and lower layer) and depth to bedrock or groundwater have been obtained by classifying the soil type map and assigning the corresponding soil texture and depth (FAO, 2001).

The values of the respective parameters of land cover (crop coefficient) and soil type (saturated and residual volumetric soil moisture content, pore size index and saturated hydraulic conductivity) were taken from the Handbook of Hydrology (Table 2.5) by Maidment (1992) and Estimation of Soil Water Properties (Table 2) by Rawls et al., (1982) respectively.

4.2.5. Digital Elevation Model

The Digital Elevation Model (DEM) used for this study is Shuttle Radar Topographic Mission (SRTM) product of 1km x 1km resolution obtained from '<https://hc.box.net/shared/1yidaheouv> website' (password: ThanksCSI!). The DEM product is resampled from version 4.1 SRTM of 90m x 90m resolution by Consultative Group for International Agricultural Research-Consortium for Spatial Information (CGIAR-CSI). The SRTM is an international project organized by the National Geospatial-Intelligence Agency (NGIA) and National Aeronautics and Space Administration (NASA) whose objective is to produce digital topographic data for 80% of the Earth's land surface (all land areas between 60° north and 56° south latitude) (CGIAR-CSI, 2011).

From the DEM map, using the 'DEM Hydro-processing' operations available in ILWIS (Maathuis and Wang, 2006) elevation related input parameters/maps used in the LISFLOOD model were derived. The input maps created are: a mask map (model boundary map), a local drainage direction map, a slope map (gradient map), an elevation map and drainage network map (used for producing channel geometry). Some of the DEM Hydro-processing operations procedures used are:

- The fill and sinks operation, which removes the local depressions with an elevation value lower than all of its 8 neighbouring pixels and increases the pit to the lowest value of its 8 neighbour pixels;
- Flow direction operation, which determines the direction of flow of water towards a neighbouring pixel having the steepest slope among the 8 neighbouring pixels;
- The flow accumulation operation, which produce the number of upstream contributing pixels of a given outlet; and
- Stream network and catchment extraction, which produces a drainage network (channels) and catchment for a given outlet (after Maathuis and Wang, 2006).

Mask map

The mask map is an area map which defines the model boundary. To avoid unexpected results and model behaviour, all maps, except channel parameters maps were defined in such way that they do not contain missing values for any pixel, which is “true” for the mask map (after Van Der Knijff and De Roo, 2008). The mask map was created by using the following PCRaster application;

Syntax: `...\mapattr [options] PCRmap1 PCRmap2....PCRmapn`

Where;

- ‘mapattr’ is operator, which generates a new PCRaster map with map attributes specified by the user, change or display location attributes of existing PCRaster map;
- ‘PCRmap1, PCRmap2 ... PCRmapn’ are user defined maps and it can be ‘Boolean’, ‘Nominal’, ‘Ordinal’, ‘Scalar’, ‘Directional’ or ‘ldd spatial; and
- ‘Options’ represents different option the user can apply (after Van Deursen and Wesseling, 1991).

Local drain direction map

A local drain direction is a network of cells produced from the elevation map (DEM) using the PCRaster operation ‘lddcreate’ (see the expression below). The operator creates an ‘ldd’ map (see Figure 4-3: ‘b’) using the 8 point pour algorithm (as in ILWIS) with flow directions from each cell to its steepest downslope neighbour, which identify the neighbour of the cell to which water will flow. Each network of cells has an integer value from 1 to 9, where value ‘5’ (in the centre) defines a cell without local drain direction (pit; see Figure 4-3: ‘a’) that defines the outlet point of a catchment (Van Deursen and Wesseling, 1991).

Syntax: `...\pcrcalc --lddin ldd.map = lddcreate(Dem.map, 1E35, 1E35, 1E35, 1E35)`

Where;

- ‘pcrcalc’ is PCRaster operation function;
- ‘--lddin’ is option used for removing pits at the edge of the map (outflow points of catchment);
- ‘ldd.map’ is the local drain direction map (output produced);
- ‘lddcreate’ operator for creating local drain direction map; and
- ‘Dem.map’ is the digital elevation model (Van Deursen & Wesseling, 1991)

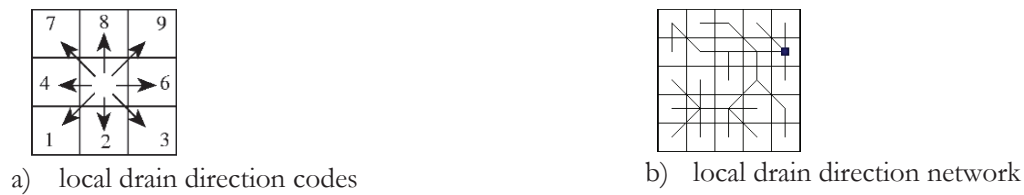


Figure 4-3: Local drain direction

Channel geometry

Input maps to the LISFLOOD model to represent channel geometry aspect are channels map, channel bottom width map [m], channel side slope map [mm^{-1}], Channel gradient [mm^{-1}], Channel length [m], channel Manning's roughness coefficient and channel bank full depth map [m]. Steps followed to obtain these input maps are:

- All the inputs, except the channel gradient and length, were prepared from the drainage network map derived using 'DEM Hydro-processing' operations available in ILWIS. For the attribute table of the drainage network map, new columns were created. Then the respective values for each input parameters (the channels bank full depth, side slope, Manning's roughness coefficient and bottom width) were provided in to the columns based on the 'Strahler order/number'. Finally, raster maps of the inputs were created using 'Polyline to Raster' tool in ArcGIS.
- The channel gradient was the result of slope map created from digital elevation model using 'slope' tool in ArcGIS, whereas, raster map of the channels length was created by classifying the local drain direction using 'reclass' tool in ArcGIS.
- All the raster maps were converted to ASCII files (*.asc) using 'Raster to Ascii' tool in ArcGIS. These files were converted to PCRaster maps using the PCRaster application 'asc2map'. The expression as given below was used to create the maps.

Syntax: *asc2map --clone clone.map -a asciifile.asc result.map*

Where;

- '--clone clone.map' is taken as clone map (this is a void map that contains the number of rows and columns, cell size, x and y coordinates and the data type);
- '-a' is option used to convert ARC/INFO ascii files;
- 'asciifile.asc' is ascii file that comes from the ArcGIS process; and
- 'result.map' is the name of the resulting PCRaster map.

4.3. Model setup

Model setup is about how the input files (maps and tables) and output files are organized and defined. Besides, it also includes how the setting files (file connecting the inputs, parameters and constants) are prepared. In the case of the LISFLOOD model there is a default model setup proposed by the model developers, where by:

- all base maps are in one directory (e.g. 'maps');
- all tables are in one directory (e.g. 'tables');
- all meteorological input maps are in one directory (e.g. 'meteo');
- all Leaf Area Index maps are in one directory (e.g. 'lai') and
- all output will be stored in one directory (e.g. 'out')(after Van Der Knijff and De Roo, 2008).

4.3.1. Model input files (parameters)

All input in the LISFLOOD model is provided as either maps of grid files in PCRaster format or tables in text file readable format. The input maps are classified in eight categories and tables are classified in two groups as presented in Table 4-2 and 4-3 respectively. Except, the meteorological variables and Leaf Area Index all other input is defined as a single map, whereas, the meteorological variables and the LAI are defined as time series maps (as map stacks). Each map represents the value of a variable at an individual time step (in this case per day). The naming of each time series map is made of 11 characters and starts with a prefix ('pr', 'et', 'es', 'e' and 'lai': see Table 4-2), and ends with the time step number. All character positions in between are filled with zeros '0' (after Van Der Knijff and De Roo, 2008). Example for naming a stack of precipitation maps is as shown below.

pr000000.007 : precipitation map at time step 7
 pr000035.260 : precipitation map at time step 35260

Table 4-2: LISFLOOD input maps (after Van Der Knijff and De Roo, 2008)

CATEGORIES	NAME/PREFIX	DESCRIPTION
Model boundary		
Mask	area.map	Boolean map that defines model boundaries
Topography		
Local direction map	ldd.map	This file contains flow directions from each cell to its steepest neighbour (with value 1-9)
Gradient	gradient.map	Slope gradient [mm ⁻¹]
Land use		
Land use	landuse.map	Map with land use classes
Forest	forest.map	Forest fraction for each cell. Values range from 0 (no forest at all) to 1 (pixel is 100% covered by forest)
Direct runoff fraction	directrf.map	Fraction urban area for each cell. Values range from 0 (no urban area at all) to 1 (pixel is 100% urban area)
Soil		
Texture 1	soiltex1.map	Soil texture class layer 1 (upper layer)
Texture 2	soiltex2.map	Soil texture class layer 2 (lower layer)
Soil depth	soildep.map	Depth to bedrock or groundwater [cm]
Channel geometry		
Channels	chan.map	Map with Boolean 1 for all channel pixels, and Boolean 0 for all other pixels on Mask Map
Channel gradient	changrad.map	Channel gradient [mm ⁻¹]
Channel Manning	chainman.map	Manning's roughness coefficient for channels
Channel length	chanleng.map	Channel length [m]
Channel bottom width	channelbw.map	Channel bottom width [m]
Meteorological variables		
Precipitation	pr	Precipitation rate [mm day ⁻¹]
EO	e	Daily potential evaporation rate free water surface [mmday ⁻¹]
ESO	es	Daily potential evaporation rate, bare soil [mmday ⁻¹]
ETO	et	Daily potential evapotranspiration rate reference crop [mmday ⁻¹]
Development of vegetation over time		

LAI	lai	Pixel-average Leaf Area Index [m ² m ⁻²]
Input/output time series		
Gauges	outlets.map	Nominal map with locations at which discharge time series are reported
Sites	sites.map	Nominal map with locations at which time series of intermediate state and rate variables are reported

Table 4-3: LISFLOOD input tables (after Van Der Knijff and De Roo, 2008)

TABLE	NAME	DESCRIPTION
Land use		
Crop coefficient	cropcoef.txt	Crop coefficient for each land use class [-]
Manning's roughness	n.txt	Manning's roughness for each land use class [-]
Soil texture		
TabThetaSat1	thetas1.txt	Saturated volumetric soil moisture content layer 1 [-]
TabThetaSat2	thetas2.txt	Saturated volumetric soil moisture content layer 2 [-]
TabThetaRes1	thetar1.txt	Residual volumetric soil moisture content layer1 [-]
TabThetaRes2	thetar2.txt	Residual volumetric soil moisture content layer2 [-]
TabLambda1	lambda1.txt	Pore size index (λ) layer 1 [-]
TabLambda2	lambda2.txt	Pore size index (λ) layer 2 [-]
TabGenuAlpha1	alpha1.txt	Van Genuchten parameter α layer 1 [-]
TabGenuAlpha2	alpha2.txt	Van Genuchten parameter α layer 2 [-]
TabKSat1	ksat1.txt	Saturated conductivity layer 1 [cmday ⁻¹]
TabKSat2	ksat2.txt	Saturated conductivity layer 2 [cmday ⁻¹]

4.3.2. The settings file

The setting file is a file where all file and parameter specifications are defined and it has an XML ('Extensible Mark-up Language') structure. The main purpose of the setting file is to link variables and parameters in the model to input and output files (maps, time series and tables) and numerical values. The settings file has four elements, where each part has its own functions. These elements are 'lfuser', 'lfoptions' and 'lfbinding'. 'lfuser' is used to define paths to all files and main model parameters; 'lfbinding' is used for defining of all individual files, and model parameters; and 'lfoptions' is used to switch on and off specific components of the model (after Van Der Knijff and De Roo, 2008).

Table 4-4: The basic structures of the setting file (after Van Der Knijff and De Roo, 2008)

<lfsettings>	Start of settings element
<lfuser>	Start of element with user-defined variables
</lfuser>	End of element with user-defined variables
<lfoptions>	Start of element with options
</lfoptions>	End of element with options
<lfbinding>	Start of element with 'binding' variables
</lfbinding>	End of element with 'binding' variables
<prolog>	Start of prolog
</prolog>	End of prolog
</lfsettings>	End of settings element

In this study the settings file was prepared by editing the template provided as one component in the LISFLOOD package. However, in order to use the template; all input maps and tables are named according to default file names (as presented in Table 4-2 and 4-3) and stored in a specific directory prepared for each of the files.

4.3.3. Output generated by the LISFLOOD

The type and amount of output to be generated from the LISFLOOD model simulation depends on the needs of the user. LISFLOOD can generate a wide variety of output, either maps (PCRaster format) or time series ASCII files. However, by default the outputs presented in Table 4-5 are generated. Besides, LISFLOOD reports maps of all state variables at the last time step of a simulation, which can be used for defining the initial conditions of a subsequent simulation (after Van Der Knijff and De Roo, 2008).

Table 4-5: The default output from LISFLOOD simulation (after by Van Der Knijff and De Roo, 2008)

Description	Units	File name
Rate variables at gauges		
channel discharge	m ³ /s	dis.tss
Numerical checks		
cumulative mass balance error	m ³	mbError.tss
cumulative mass balance error, expressed as mm water slice (average over catchment)	mm	mbErrorMm.tss
number of sub-steps needed for gravity-based soil moisture routine	-	steps.tss

4.4. Initialization of the model

Like other hydrological models, LISFLOOD needs to have an estimate of the initial approximation of its internal state variables. According to Van Der Knijff and De Roo, (2008) the LISFLOOD model has two types of initialization options, which are ‘initial state of all state variables are known’ or ‘unknown’. For this study the initial state of all state variables are unknown. So, to initialize the model, a warm-up period was selected that started two years prior to the actual simulation. The meteorological and LAI maps used for model initialization were copied from the year 2007 and 2008. The simulation was started at the end of the dry season (where the catchment is in steady state response mode) to get the starting state of the actual simulation period (1st of January 2007 up to 31st December of 2009).

As suggested by Van Der Knijff and De Roo, (2008), prior to the warm up period the internal state variables; the initial amount of water on the soil surface, interception storage and storage in the upper groundwater zone were set to zero, and the days since last rainfall event was set to 1. On the other hand, in LISFLOOD the following parameters are internally initialized using special initialization methods whereby the initial values of each of the variables are set to a special ‘bogus’ value of ‘-9999’. These variables are:

- Initial cross-sectional area of water in channels;
- Initial soil moisture content of upper and lower soil layer;
- Initial water in lower groundwater zone.

Initialization of the lower groundwater zone

The limiting factor to initialize the lower groundwater zone in the model is the average residence time of the water. The lower ground water response is relatively slow compared to upper layer soil moisture

content and therefore, needs a long warm-up period to avoid unrealistic trends in simulation. However, in order to avoid the need for excessive warm-up periods, LISFLOOD is capable of calculating a ‘steady-state’ storage amount for the lower groundwater zone (after Van Der Knijff and De Roo, 2008).

In this study from the two ways (‘prior estimate of average recharge’ and the ‘pre-run to calculate average recharge’) of initialization procedure suggested by Van Der Knijff and De Roo, (2008), ‘pre-run’ procedure was used. In this procedure, the lower groundwater zone was initialized using “pre-run” method, which is used to calculate the average inflow into the lower zone. This average inflow is reported as a map, which was then used in the actual run.

4.5. Model calibration

Model uncertainties depend on model structure, boundary and initial condition, parameters and meteorological-forcing terms. However, considering all these mentioned uncertainty source to come up with a well calibrated model that efficiently simulates the catchment response is very complex. So, to reduce model calibration complexity, most commonly only parameter optimization is used (modified after Rientjes, 2004).

In addition of selecting the calibration parameters, also performance indicators (objective functions) and a calibration method needs to be selected (automated or trial and error) which play an important role in the calibration process. Various kinds of objective functions are available for performance and uncertainty assessment for model calibration process. Moriasi, et al., (2007) have presented different kinds of objective functions used for model evaluation in simulating the catchment response. From those presented the Root Mean Square Error (RMSE; optimum value is 0), the Nash-Sutcliffe coefficient of Efficiency (NSE: range between $-\infty$ to 1, optimum value is 1) and the Relative Volumetric Error (RV_e : optimum value is 0) was selected and used in this study. The equations used are presented below.

$$RMSE = \sqrt{\frac{\sum_{i=1}^n (X_{obs,i} - X_{model,i})^2}{n}} \quad (4.4)$$

$$RV_e = \left(\frac{\sum_{i=1}^n X_{model,i} - \sum_{i=1}^n X_{obs,i}}{\sum_{i=1}^n X_{obs,i}} \right) \times 100 \quad (4.5)$$

$$NSE = 1 - \frac{\sum_{i=1}^n (X_{obs,i} - X_{model})^2}{\sum_{i=1}^n (X_{obs,i} - X_{obs,mean})^2} \quad (4.6)$$

Where;

- $X_{obs,i}$ is observed values;
- $X_{obs,mean}$ is mean observed value; and
- X_{model} is modeled values at time or place i .

In LISFLOOD some of the parameters can be obtained from field measurement, whereas some parameters can be obtained by calibration. There are five parameters (Table 4-6) that need to be estimated by calibration in LISFLOOD model (after Van Der Knijff and De Roo, 2008 and Feyen et al., 2007). In this study a trial and error calibration was performed for the year 2007 and 2008. Finally, the model performance is validated using observed stream flow of the year 2009.

Table 4-6: Calibration parameters of the LISFLOOD model (Source: Feyen et al., 2007)

Parameters	Upper and lower limit	Description
Upper zone time constant (UZTC)	1 – 10	control the amount and timing of outflow upper groundwater reservoirs
Lower zone time constant (LZTC)	10 – 5000	control the amount and timing of outflow lower groundwater reservoirs
Ground water percolation value (GWPV)	0 – 0.5	controls the flow from the upper to the lower groundwater zone
Xinanjiaog parameter b (Xb)	0.05 – 0.5	controls the fraction of saturated area within a grid cell that is contributing to runoff
Power preferential bypass flow (PPBF)	5 – 15	relates preferential flow with the relative saturation of the soil

4.6. ASCAT surface soil moisture

Soil moisture product retrieved from Advanced Scatterometer on-board of MetOp (Meteorological Operational satellite programme) having 12.5km grid spacing (level 2) and a daily temporal resolution, disseminated via GEONETCast, was selected to identify wetness distribution in the study area. The processing algorithm for retrieval is given in the ‘ASCAT Soil Moisture Product Handbook’ prepared by Vienna University of Technology (Bartalis et al., 2008).

Reports on validation of ASCAT surface soil moisture product using model output and in situ measurement for different areas indicated good correlation between ASCAT and in situ measurement and/or model output (Brocca et al., 2010; Albergel et al., 2012). Brocca et al. (2010) assessed the accuracy of 25 km ASCAT derived saturation degree product by using in situ observations and the outcomes of a soil water balance model for three sites located in an inland region of central Italy and has found good correlation. For this specific study, the surface soil moisture from the satellite product (ASCAT) was validated using *in-situ* measured soil moisture of shallow soil depth (0-10cm) using a Theta probe during field visit. Root mean square error (RMSE) was used for validation.

4.7. Flood prone area(s) verification using water level simulation in LISFLOOD

According to the report by the Ethiopian ministry of Energy and Water (MoEW) and Halcrow (2006), there are some places (Becho, Wonji and Melka Werer floodplains) in the Awash River Basin which are known to flood every year (see Figure 3-3). The flooding that occurs at those locations inundates the floodplain and stays for more than two to three weeks and up to a month (especially in the Becho flood plain).

To verify the occurrence of flood on the flood prone area(s) using the model, simulation of water level in the channel at those specific places were done. It has been assumed that, if there exists overtopping of water at those specific location while simulating for a certain period (wet season: July-September), then the place(s) is/are identified as ‘flood prone area(s)’. Figure 4-4 below shows how the water level simulation would look like when the water in the channel exceeds the bank full depth and evenly distributed on the floodplain. Water that overtops the channel bank is homogeneously distributed over the pixel where the channel is located.

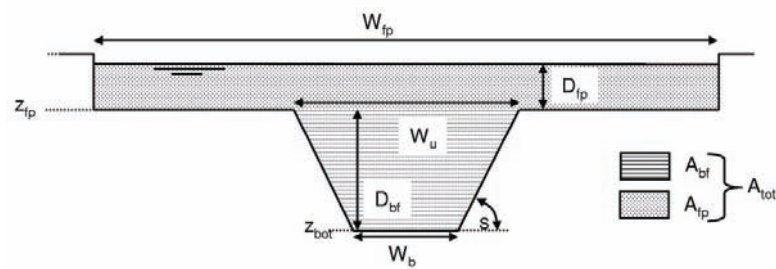


Figure 4-4: Geometry of channel cross-section (Source: Van Der Knijff and De Roo, 2008)

Where;

- W_b : channel bottom width; W_u : channel upper width; Z_{bot} : channel bottom level; Z_{fp} : floodplain bottom level; S : channel side slope; W_{fp} : floodplain width; A_{bf} : channel cross-sectional area at bank full depth; A_{fp} : floodplain cross-sectional area; D_{bf} : bank full channel depth, D_{fp} : depth of water on the floodplain

To simulate water levels in LISFLOOD a map indicating the ‘floodplain width’ is required as input. The flood plain width used to simulate water level in this study was 1000m. The water level simulation was done for the period 2007 – 2009. The water levels can be reported as time series (at the gauge locations that are also used for reporting discharge), or as maps. The time series report on water level simulation of wet seasons were used to indicate the flood prone areas.

4.8. Standardized Precipitation Index

The Standardized Precipitation Index is simply the difference of precipitation from the mean for a specified time period divided by the standard deviation (McKee et.al., 1993). Negative SPI value indicates dryness and positive indicates wetness as categorized in Table 4-7. The SPI is calculated using the following formula:

$$SPI = \frac{(X_i - X_{mean})}{\sigma} \quad 4.7$$

Where;

- X_i is the accumulated daily (monthly) precipitation observation, X_{mean} is the mean daily (monthly) precipitation, and σ is the standard deviation.

Table 4-7: Category of SPI (adapted from McKee et al., 1993)

SPI Values	Categories
2.0 and above	Extremely wet
1.5 to 1.99	Very wet
1.0 to 1.49	Moderately wet
-0.99 to 0.99	Near normal
-1.0 to -1.49	Moderately dry
-1.5 to -1.99	Severely dry
-2.0 and less	Extremely dry

4.9. Topographic Wetness Index

Topographic wetness index (TWI) is developed to quantify the effect of local topography on hydrological processes and for modelling the spatial distribution of soil moisture (wetness) and surface saturation. It is originally developed by Beven and Kirkby, (1979) and formulated as:

$$TWI = \ln\left(\frac{As}{\tan\beta}\right) \quad 4.8$$

Where;

- As is the upslope contributing area per unit contour length defined as horizontal pixel dimension (or Specific Catchment Area, SCA) and $\tan\beta$ is local slope in the steepest down slope direction of the terrain in degrees. TWI is topographic wetness index which indicate the tendency of water to accumulate at any point in the catchment (in terms of 'a') and the tendency for gravitational force to move that water downslope (in terms of $\tan\beta$).

4.10. Combining SPI and TWI

In this study the SPI and TWI maps were combined to produce an index which indicates source areas for flood (see Figure 4-5). The combined index was made to have an information on areas receiving above normal rainfall (attributed from SPI) and effect of topography (attributed from TWI). TWI was calculated from the SRTM DEM of 1km x 1km resolution. The value of the index ranges from 5 to 30 for the study area. Areas with high TWI (in this case ≥ 12.5), which are located in the vicinity of the main river were excluded. This is done only to include the effect of the upstream areas where most of the rainfall occurs. On the other hand, the daily SPI maps were calculated from CMORPH rainfall product of the period 2006 to 2010. The SPI maps of the wet period (June – August) for the years 2007, 2008 and 2009 were smoothed by applying moving average of 5 days to identify possible window(s) of time indicating high SPI values. The positive SPI values were only considered. Then the values of both indices were normalized between 0 and 1. Finally, both indexes were combined by giving equal weight to produce combined index (flood index) maps. The following formula was used to combine both indexes to yield the combined index map.

$$FI = w1(TWI) + w2(SPI) \quad 4.9$$

Where;

- FI = flood index map; w1, w2 = weight given for TWI and SPI respectively (=0.5; assuming equal influence); TWI = Topographic Wetness Index; and SPI = Standard Precipitation Index

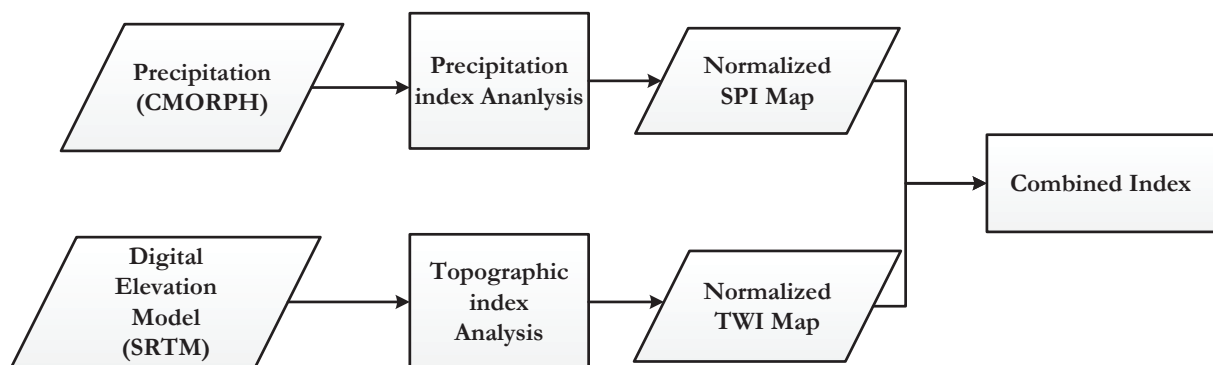


Figure 4-5: Flowchart for combining SPI and TWI

5. RESULT AND DISCUSSION

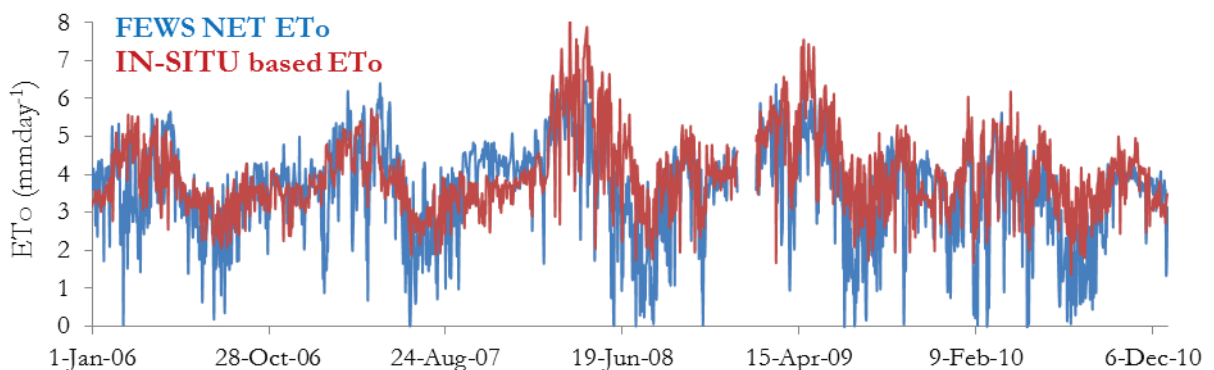
5.1. Reference evapotranspiration (ET_o) analysis

In this section the FAO Penman-Monteith based ET_o estimates using *in-situ* measured meteorological variables and the ET_o estimates from FEWS NET using meteorological variables from Global Data Assimilation System were compared. The comparison was for 12 stations (Figure 3-3) and covers 5 years of recordings (2006 – 2010). ET_o estimates were extracted from the FEWS NET ET_o product which spatially corresponded with the *in-situ* ET_o estimates. In two instances, a single pixel encompassed several stations. These stations are Adama, Matahara, Abomsa and Kulumsa (AMAK) as well as Shola Gebiya and Debrebrihan (ShDb).

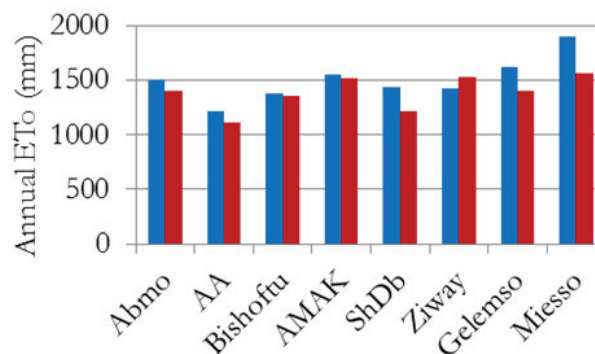
The FEWS NET ET_o estimates during wet seasons are underestimated (except at Mieso station) compared to *in-situ* based ET_o estimates, whereas, the average annual accumulated ET_o from FEWS NET is 64mm higher than the *in-situ* based ET_o. The average root mean square error (RMSE) found was 1.2mmday⁻¹ (see Table 5-1). Figure 5-1 (a) below shows the daily variation of FEWS NET and *in-situ* based ET_o estimates at the Bishoftu meteorological station for the period 2006 - 2010 and (b) shows the annual FEWS NET and *in-situ* based ET_o estimates at all stations for the period 2007. Graphs of at remaining stations are found in Annex A.

Table 5-1: RMSE values at respective stations. RMSE for AMAK and ShDb were calculated using the average ET_o at the respective stations.

2006 up to 2010	Ambo	Addis Ababa (AA)	Bishoftu	AMAK	ShDb	Ziway	Gelemso	Mieso
RMSE [mmday ⁻¹]	1.2	1.1	1.2	1.0	1.1	1.1	1.4	1.3
Average = 1.2								



a)



b)

Figure 5-1: (a) Daily variation of FEWS NET and *in-situ* based ETo estimates at Bishoftu station (2006 – 2007) and (b) annual FEWS NET and *in-situ* based ETo estimates at respective station for the year 2007

Both ETo estimates were used as meteorological forcing in the model simulation. To use the *in-situ* based ETo as input meteorological forcing in the model, a weighted distance average interpolation method was applied. The performance of the interpolation technique was checked by applying a cross validation procedure, whereby ETo was interpolated using 10 out of the 12 stations in the study area. The interpolated values were compared with ETo values of the omitted stations' (Adama and Miesso). RMSEs of 1.30mmday^{-1} and 0.82mmday^{-1} were found at Adama and Miesso respectively.

5.2. Rainfall data analysis and comparison

Satellite rainfall estimate products CMORPH (2006 – 2010) and MPE (2010) were compared to measured rainfall from the 12 stations. The objective of this comparison was to be able to validate satellite derived rainfall data. In this study simple analyses have been undertaken based on pair-wise comparisons of the gauge measured rainfall and the satellite estimates. The comparison was based on annual rainfall totals at each station with analysis of the time series of daily rainfalls and simple statistics (the annual cumulative difference). No further statistical measures of fit have been used during this phase of the study, although additional measures may be useful prior to usage of the data in the model.

The $0.25\text{degree} \times 0.25\text{degree}$ (CMORPH) and $3\text{km} \times 3\text{km}$ (MPE) grid squares extracted rainfall values were compared with measured rainfall from station(s) that are located within the corresponding pixels. Figure 5-2 (a), (b) and (c) shows the accumulated rainfall measurement from stations and accumulated rainfall estimates from the corresponding CMORPH pixels for the period 2007, 2008 and 2009 respectively. The accumulated values in the figure represent the sum of accumulated rainfall values from all stations where the CMORPH underestimates. Figure 5-2 (d), (e) and (f) shows the annual rainfall (CMORPH and station) at each station separately, for the period 2007, 2008 and 2009 respectively. The accumulated CMORPH rainfall estimates of the year 2007 and 2009 underestimated compared to the measured rainfall from station, whereas in 2008 the difference between the station and CMORPH rainfall estimate is less compared to the difference for the year 2007 and 2009 (Figure 5-2 a, b and c). The CMORPH annual rainfall estimates is lower than the measured rainfall at all stations except Abomsa, Gelemso, Miesso and Ziway for the period 2007 and Gelemso and Miesso for the period 2009 (Figure 5-2 d and f).

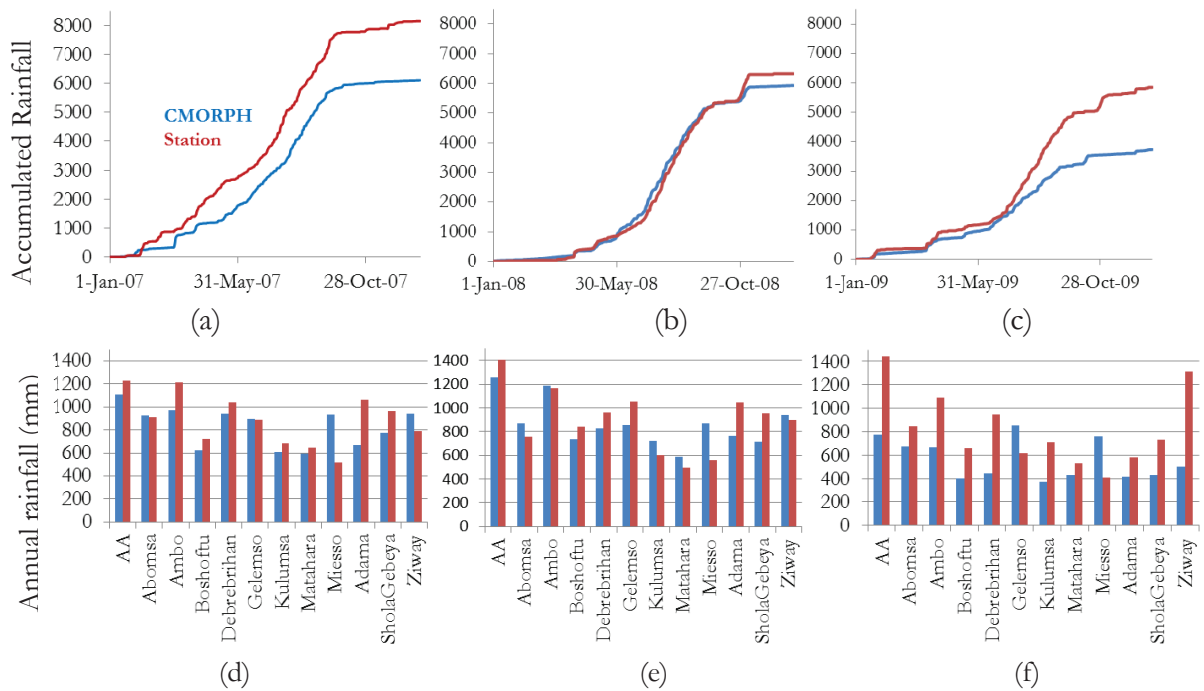


Figure 5-2: CMORPH and station rainfall data comparison

The Multi-sensor Precipitation Estimate from EUMETSAT of the year 2010 was compared to *in-situ* rainfall. The average annual difference (12 stations) is 246mm yr^{-1} for CMORPH and 669mm yr^{-1} for MPE. The MPE underestimation result agrees with the result from Samain and Heinemann (2007). According to their analysis, MPE product is not suitable to locate rain-pattern correctly for the study area, since correlation of IR derived rain rate and the SSM/I rain rate is very low. Figure 5-3 (a) shows the accumulated rainfall measurement from stations and accumulated rainfall estimates from the corresponding MPE pixels with the stations for the period 2010. Figure 5-2 (b) shows the annual rainfall (MPE and station) at each station separately, for the period 2010.

MPE has a larger underestimation than CMORPH and the record of the rainfall from MPE is only available for the year 2009 and 2010 (available processed daily data at ITC). However, the observed stream flow records are only available until 2009, so CMORPH was selected for model simulation.

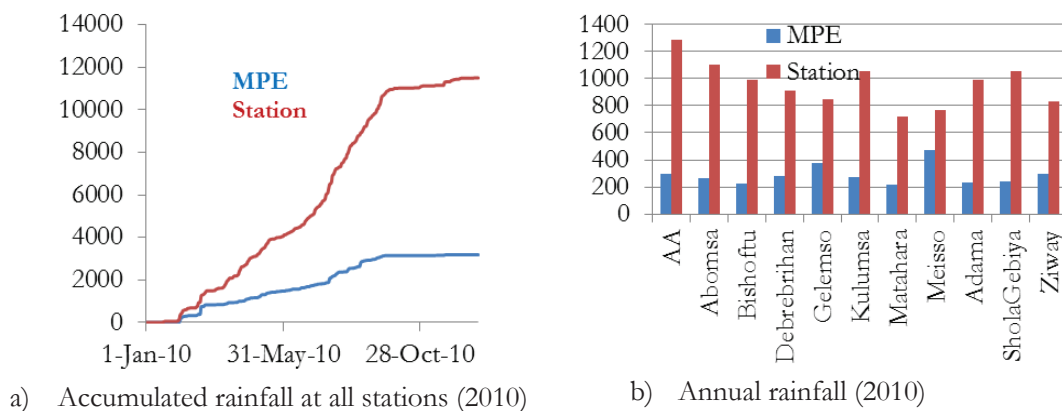


Figure 5-3: MPE and station rainfall data comparison

CMORPH was used to simulate stream flow. However, the simulated hydrograph for the period 2007 and 2009 does largely deviates from the observed hydrograph which is due to the underestimation of the

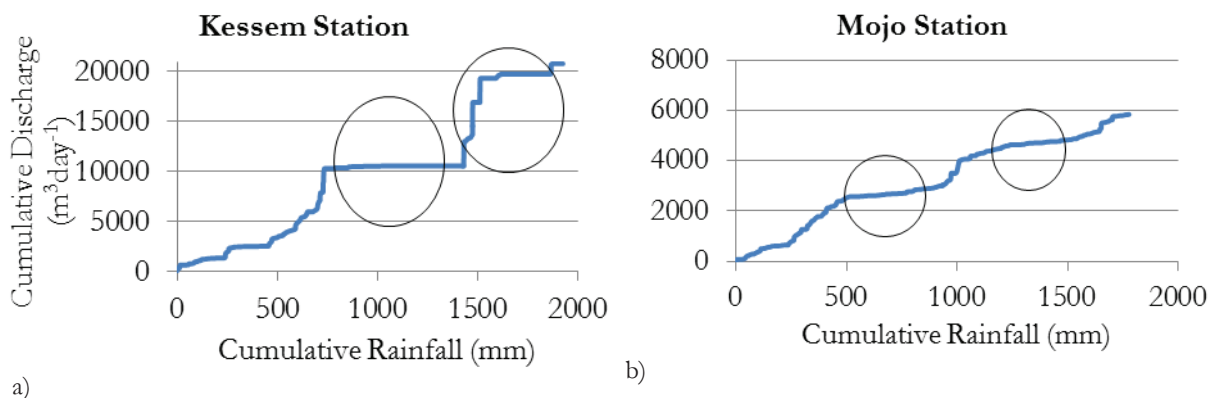
CMORPH rainfall estimate. Therefore, a correction factor was applied to correct the CMORPH rainfall estimates, assuming that the gauge rainfall data is accurate (representative of the area). Consequently, the CMORPH rainfall data of the respective years were multiplied by a correction factor. In Table 5-2 below the correction factors for the 2006 – 2010 are presented.

Table 5-2: Correction factor applied for the respective year

Year	Accumulated Rainfall of all stations [mm]		Ratio [Station/CMORPH]
	CMORPH	Station	
2006	7609	10805	1.42
2007	7910	10600	1.34
2008	10322	10745	1.04
2009	6650	10041	1.51
2010	7273	10255	1.41

5.3. Selection of observed hydrograph for model calibration and validation

The selection of gauges having continuous records for model calibration and validation was challenging, since observed stream flow hydrographs (see Figure 3-4) are not always complete and/or reliable. In order to check the reliability of the data, double mass curve procedure was used. To produce the double mass curve the accumulated observed stream flow discharge was plotted against accumulated rainfall from CMORPH up stream of the discharge measuring gauges. Figure 5-4 shows the double mass curve of two stations on tributaries' reach (Kessem and Mojo) and two stations on the main reach (Melka Hombole and Wonji). The double mass curve plot of the stations indicates breaks in slope. These breaks probably are due to changes in the method of data collection or to physical changes that affect the relation. For instance, at Kessesem station the increase in rainfall has not shown an effect on the observed stream flow hydrograph, because there is no record of discharge for the period where there is rainfall record and vice versa (see the circles on Figure 5-4 a). Moreover, the change in slope is not the same (see the circles on Figure 5-4). The calibration and validation of the model is performed using observed discharge at Melka Hombole station, because the observed discharge at this station is better than the other stations (qualitative: visualization see Figure 5-5).



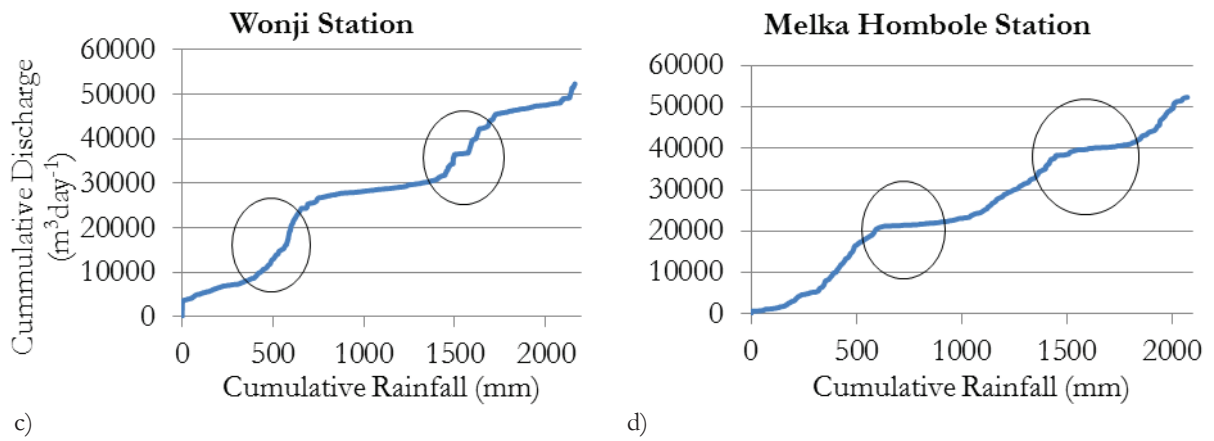


Figure 5-4: Double mass curve of cumulative observed discharge vs. satellite rainfall

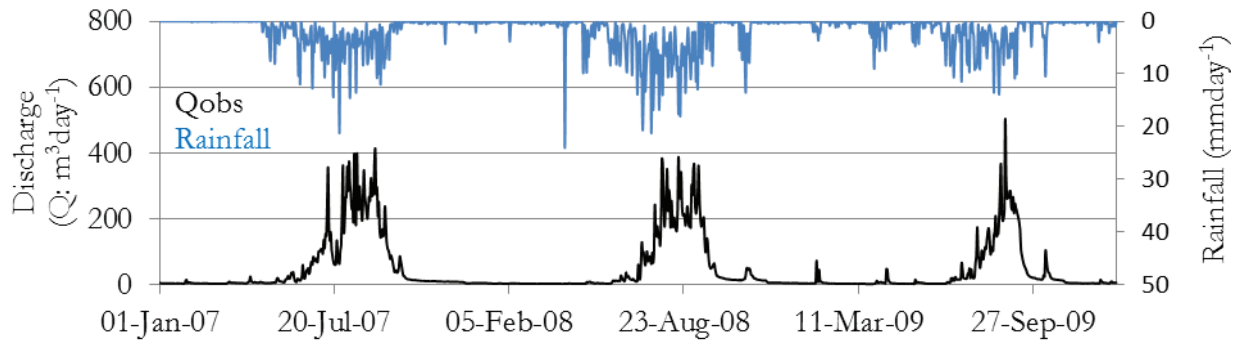


Figure 5-5: Observed stream flow at Melka Hombole station used for calibration and validation of the model

Figure 5-6 below shows the distribution of sub-catchments that used for the double mass curve analysis.

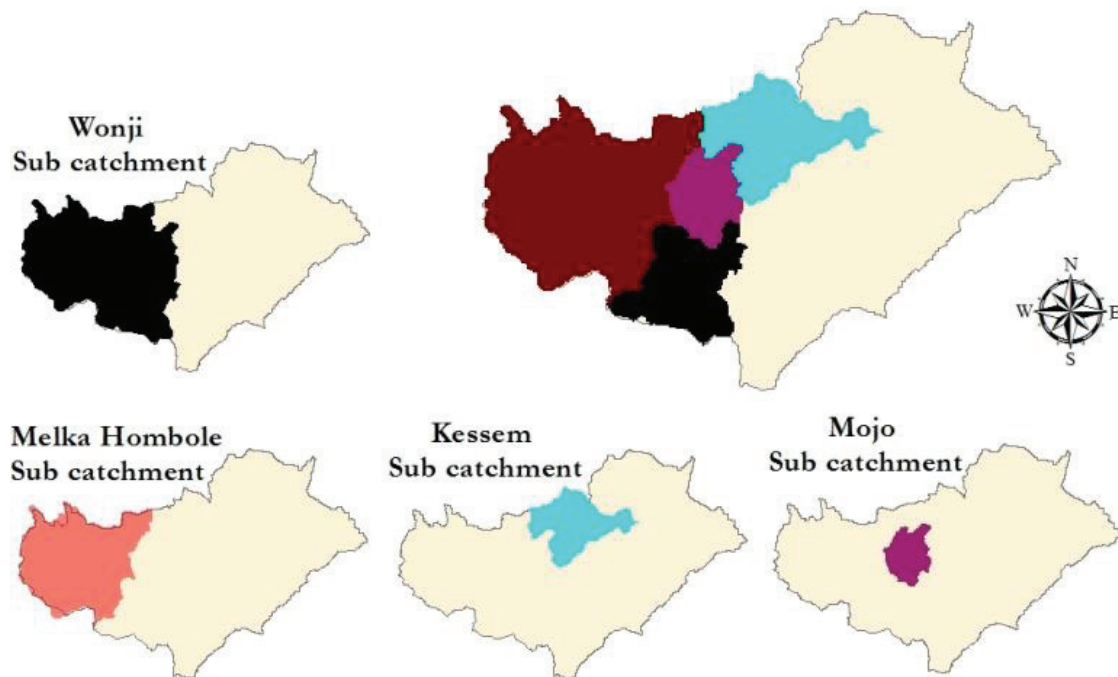


Figure 5-6: Sub catchments for which the double mass curve analysis was applied

5.4. Sensitivity analysis of LISFLOOD input parameters

Sensitivity of the five parameters (UZTC, LZTC, GWPV, Xb and PPBF (see Table 4-6)) of the LISFLOOD model have been evaluated using selected value ranges of parameters as presented in Table 5-3. The sensitivity analysis was done by changing one parameter value at a time and keeping the other parameters constant. For each of the parameters five different values were used to assess the sensitivity. These values are highlighted in red (Table 5-3). Table 5-3 shows the parameter values and objective functions obtained for the sensitivity analysis. In the table, the combinations of parameters that gave the best objective function values and showed a best fit between the observed and simulated hydrographs are in bold and italic.

Table 5-3: Parameters and objective functions for sensitivity analysis

RUN	Parameters					Objective Functions		
	LZTC	GWPV	UZTC	Xb	PPBF	RMSE	NSE	RVE
	[days]	[mmday ⁻¹]	[days]	[-]	[-]	[m ³ s ⁻¹]	[-]	[%]
1	<i>10</i>	<i>0.08</i>	<i>3</i>	<i>0.05</i>	<i>8</i>	<i>55.55</i>	<i>0.71</i>	<i>0.27</i>
2	<i>50</i>	<i>0.08</i>	<i>3</i>	<i>0.05</i>	<i>8</i>	<i>55.29</i>	<i>0.72</i>	<i>0.27</i>
3	<i>500</i>	<i>0.08</i>	<i>3</i>	<i>0.05</i>	<i>8</i>	<i>54.89</i>	<i>0.72</i>	<i>0.27</i>
4	<i>2000</i>	<i>0.08</i>	<i>3</i>	<i>0.05</i>	<i>8</i>	<i>54.9</i>	<i>0.72</i>	<i>0.27</i>
5	<i>5000</i>	<i>0.08</i>	<i>3</i>	<i>0.05</i>	<i>8</i>	<i>54.9</i>	<i>0.72</i>	<i>0.27</i>
6	50	<i>0</i>	3	0.05	8	55.55	0.71	0.27
7	<i>50</i>	<i>0.08</i>	<i>3</i>	<i>0.05</i>	<i>8</i>	<i>55.29</i>	<i>0.72</i>	<i>0.27</i>
8	50	<i>0.2</i>	3	0.05	8	54.75	0.72	0.26
9	50	<i>0.4</i>	3	0.05	8	53.94	0.73	0.26
10	50	<i>0.5</i>	3	0.05	8	53.6	0.73	0.26
11	50	0.08	<i>1</i>	0.05	8	58.79	0.68	0.27
12	<i>50</i>	<i>0.08</i>	<i>3</i>	<i>0.05</i>	<i>8</i>	<i>55.29</i>	<i>0.72</i>	<i>0.27</i>
13	50	0.08	<i>5</i>	0.05	8	54.6	0.72	0.27
14	50	0.08	<i>7</i>	0.05	8	55.27	0.72	0.26
15	50	0.08	<i>10</i>	0.05	8	57.22	0.7	0.26
16	<i>50</i>	<i>0.08</i>	<i>3</i>	<i>0.05</i>	<i>8</i>	<i>55.29</i>	<i>0.72</i>	<i>0.27</i>
17	50	0.08	3	<i>0.2</i>	8	55.4	0.72	0.27
18	50	0.08	3	<i>0.3</i>	8	55.88	0.71	0.27
19	50	0.08	3	<i>0.4</i>	8	56.32	0.71	0.27
20	50	0.08	3	<i>0.5</i>	8	57.14	0.7	0.28
21	50	0.08	3	0.05	<i>1</i>	103.84	0	1.23
22	50	0.08	3	0.05	<i>5</i>	57.33	0.7	0.38
23	<i>50</i>	<i>0.08</i>	<i>3</i>	<i>0.05</i>	<i>8</i>	<i>55.29</i>	<i>0.72</i>	<i>0.27</i>
24	50	0.08	3	0.05	<i>10</i>	54.45	0.73	0.22
25	50	0.08	3	0.05	<i>15</i>	52.99	0.74	0.15

The graphs and explanation of the effect of each parameter on the simulated hydrograph are discussed further below.

5.4.1. Effects of the Lower Zone Time Constant (LZTC) parameter

The ‘Lower Zone Time constant’ (LZTC) parameter controls the amount and timing of outflow from the lower groundwater reservoirs. Equation 5.1 shows the formula used in the model. It was impossible to distinguish the different discharge rates simulated from each LZTC according the objective functions values (see Table 5-3). However, the change in this parameter has shown effect on the base flow (see the zoomed part of the hydrograph in Figure 5-7).

$$Q_{lz} = \frac{1}{T_{lz}} LZ \Delta t \quad 5.1$$

Where;

- Q_{lz} = discharge from the Lower zone ground water [m³s⁻¹];
- T_{lz} = a reservoir constant (Lower Zone Time Constant-LZTC) [days];
- LZ = the amount of water that is stored in the Lower zone groundwater [mm];
- Δt is change in time (Van Der Knijff and De Roo, 2008) [day].

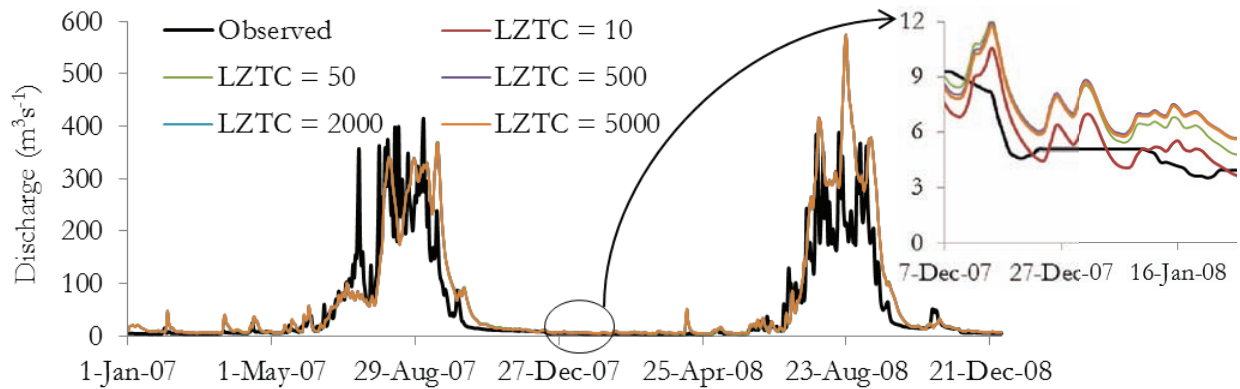


Figure 5-7: Sensitivity of the model to change in Lower Zone Time Constant parameter

5.4.1. Effects of the Groundwater Percolation Value (GWPV) Parameter

The ‘Ground Water Percolation value’ (GWPV) is a user-defined value that can be used as a calibration constant. It controls the flow from the upper to the lower groundwater zone. An increase in this parameter value resulted in an increase of base flow during the dry season (see the zoomed part of the hydrograph in Figure 5-8). The GWPV value that gave best objective function value suggesting a best fit of the observed and simulated hydrograph is ‘0.08’ for this study.

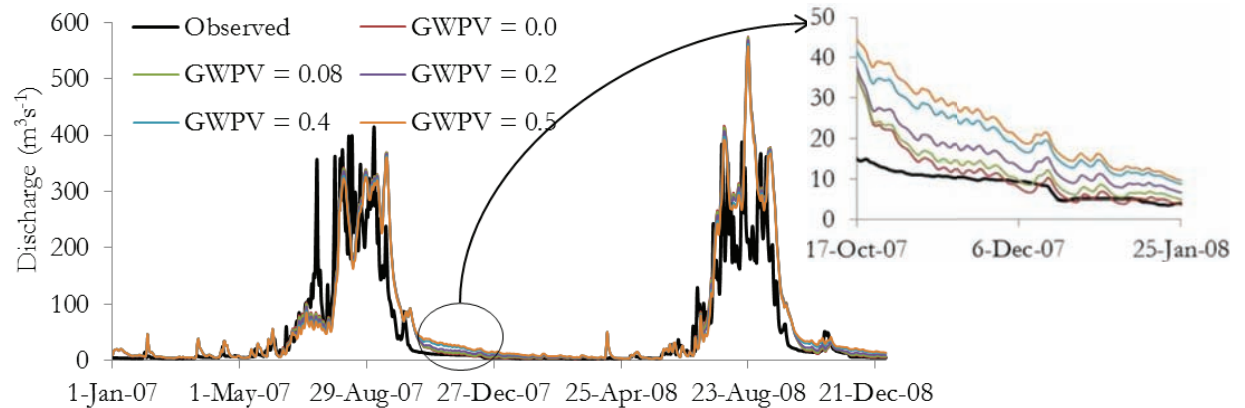


Figure 5-8: Sensitivity of the model to changes in the Groundwater Percolation Value parameter

5.4.2. Effects of the Upper Zone Time Constant (UZTC) parameter

The change in ‘upper zone time constant’ (UZTC: control the amount and timing of outflow from the upper groundwater reservoirs) has affected the peak and the recession part of the hydrograph (see Figure 5-9). As the UZTC value increases the peak flow decreases and the slope of the recession limb becomes gentler. This is because the parameter is formulated in such a way that it is inversely proportional to the discharge from the upper zone groundwater (see Equation 5.2). For this study The UZTC value of ‘3’ gave better objective functions and showed best fit of the observed and simulated hydrograph compared to the values used.

$$Q_{uz} = \frac{1}{T_{uz}} UZ \Delta t \quad 5.1$$

Where;

- Q_{uz} = discharge from the Lower zone ground water [m³s⁻¹];
- T_{uz} = a reservoir constant (Upper Zone Time Constant-UZTC) [days];
- LZ = the amount of water that is stored in the Lower zone groundwater [mm];
- Δt = change in time (Van Der Knijff and De Roo, 2008) [day].

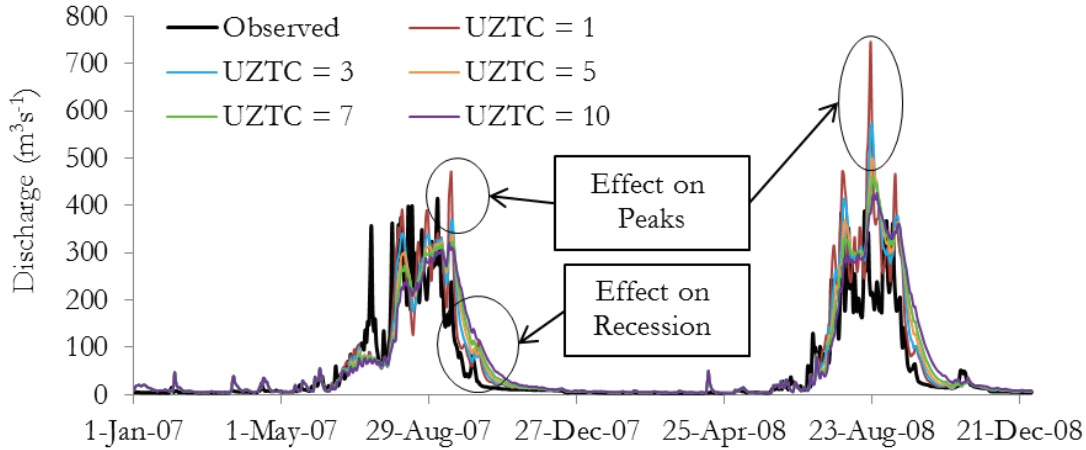


Figure 5-9: Sensitivity of the model to changes in the Upper Zone Time Constant parameter

5.4.3. Effects of the Power Preferential Bypass Flow (PPBF) parameter

An empirical shape parameter (PPBF) is used as a power function relating preferential flow with the relative saturation of the soil (after Van Der Knijff and De Roo, 2008). The sensitivity analysis result indicated that the PPBF parameter affects the quick flow. The peak flow decreases as the parameter value increases. The PPBF value of 1 showed unrealistic response of the catchment where by the soil matrix captures no rainfall and water is immediately discharged from the catchment (see Figure 5-10). This could indicate that the parameter values should not be less than 5 as suggested by Feyen et al., (2007). PPBF value of ‘8’ gives best performance indicators as shown in Table 5-3.

$$D_{pref,gw} = W_{av} \left(\frac{w_1}{w_{s1}} \right)^{PPBF} \quad 5.3$$

Where;

- $D_{pref,gw}$ = the amount of preferential flow per time step [mm];
- W_{av} = the amount of water that is available for infiltration [mm];
- w_{s1} and w_1 = the maximum and actual moisture in the upper soil layer, respectively [mm];
- PPBF = an empirical shape parameter (PPBF parameter) (Van Der Knijff and De Roo, 2008) [-].

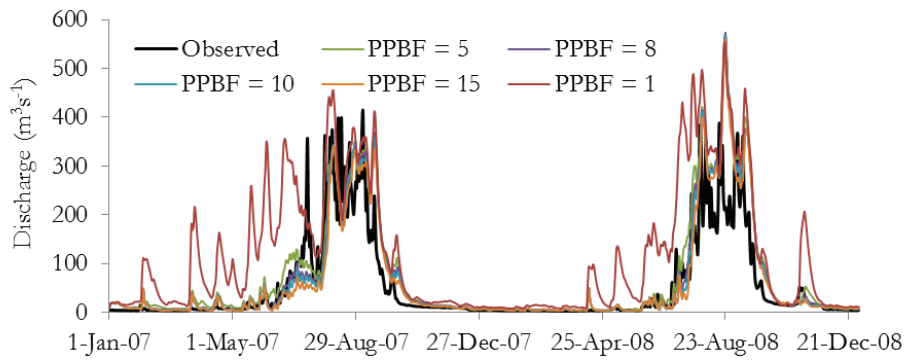


Figure 5-10: Sensitivity of the model to changes in the Power Preferential Bypass Flow parameter

5.4.4. Effect of Xinanjiang parameter 'b' (Xb)

The Xinanjiang parameter b (X_b) is an empirical shape parameter used for simulation of infiltration. It controls the fraction of saturated area within a grid cell that is contributing to surface runoff and inversely related to infiltration (after Van Der Knijff and De Roo, 2008). The increase in X_b parameter resulted in an increase in peak flow, though the differences of the obtained peaks are relatively small compared to each other (see the zoomed part of the hydrograph in Figure 5-11). X_b value of '0.05' gives best performance indicators as shown in Table 5-2.

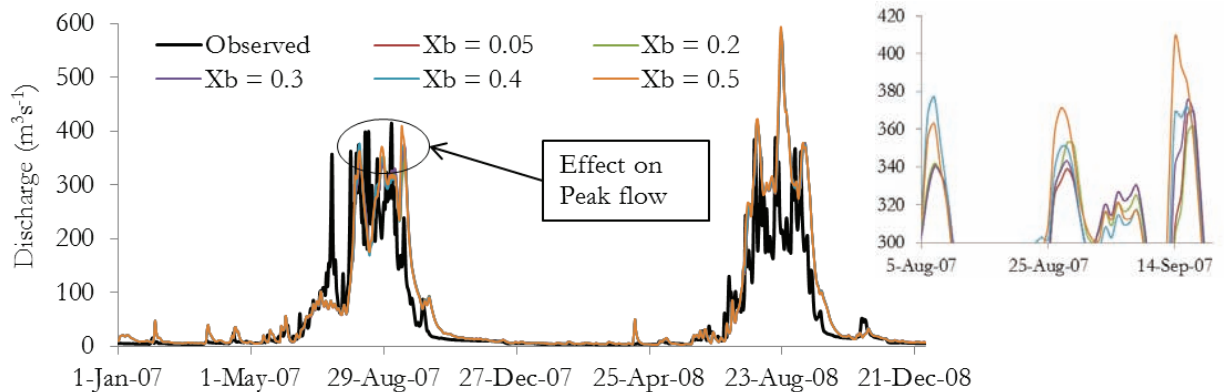


Figure 5-11: Sensitivity of the model to changes in the Xinanjiang parameter 'b'

5.5. Calibration and validation results

A trial and error procedure was used to calibrate the model using the parameters in the Table 4-6. In the calibration, qualitative (visualization) and quantitative (objective functions) analysis were performed. The observed and simulated stream flow hydrographs are compared and adjustments of calibration parameters were made to improve the match between the observed and simulated hydrographs. Prior of calibration, the model was initialized by applying warm-up period of two years.

Calibration was performed for years 2007 and 2008, whereas 2009 was used for validation. Figure 5-12 shows the result of the calibration and validation process. In the year 2008 the simulated peak flow (encircled green) is higher than the observed peak flow, whereas in the 2009 the reverse has happened. On the other hands, the simulation result in 2007 does not fit the first peak in the observed hydrograph. The optimized calibration parameters with the respective model performance indicators (RMSE, NSE and RVe) are presented in Table 5-4 below.

Table 5-4: Optimized parameter and objective function values for calibration and validation period

PARAMETERS					OBJECTIVE FUNCTIONS					
					Calibration			Validation		
UZTC	LZTC	GWPV	Xb	PPBF	RMSE	NSE	RVe	RMSE	NSE	RVe
[days]	[days]	[mmday ⁻¹]	[-]	[-]	[m ³ s ⁻¹]	[-]	[%]	[m ³ s ⁻¹]	[-]	[%]
3	10 - 500	0.08	0.05	8	55.29	0.72	0.27	29.37	0.82	21.07

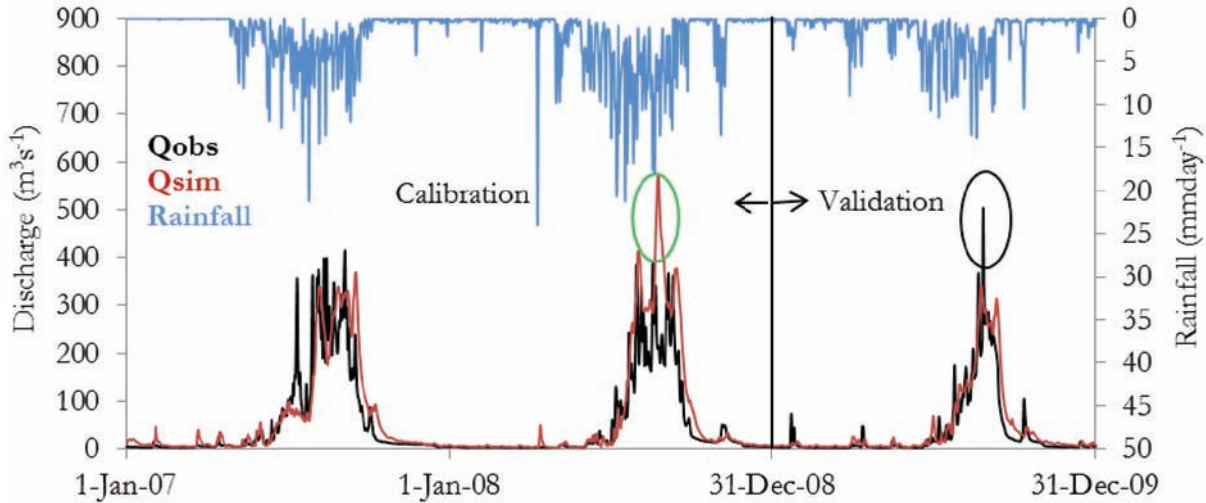


Figure 5-12: Simulated and Observed hydrograph for the period 2007 – 2009 at Melka Hombole gauge station

5.6. Simulation result using FEWS NET and in-situ based ETo

Simulation using satellite based ETo (FEWS NET) and *in-situ* based ETo was done for the period of 2007 – 2009. The result shows that the peak flow decrease (cyan coloured rectangular box; Figure 5-13) and the recession part of the base flow increased (see the red coloured oval; Figure 5-13) when *in-situ* based ETo was used as a forcing term. The higher peak flow for FEWS NET ETo is probably due to the underestimation of FEWS NET ETo during the wet season (see Figure 5-1 (a)). A lower ETo estimate results in lower extraction of water from the catchment which leads to higher peak stream flow for FEWS NET. The lower estimate for the peak flow using *in-situ* based ETo leads to a delay in the discharge response, which in turn leads to a higher base flow in the recession part of the hydrograph.

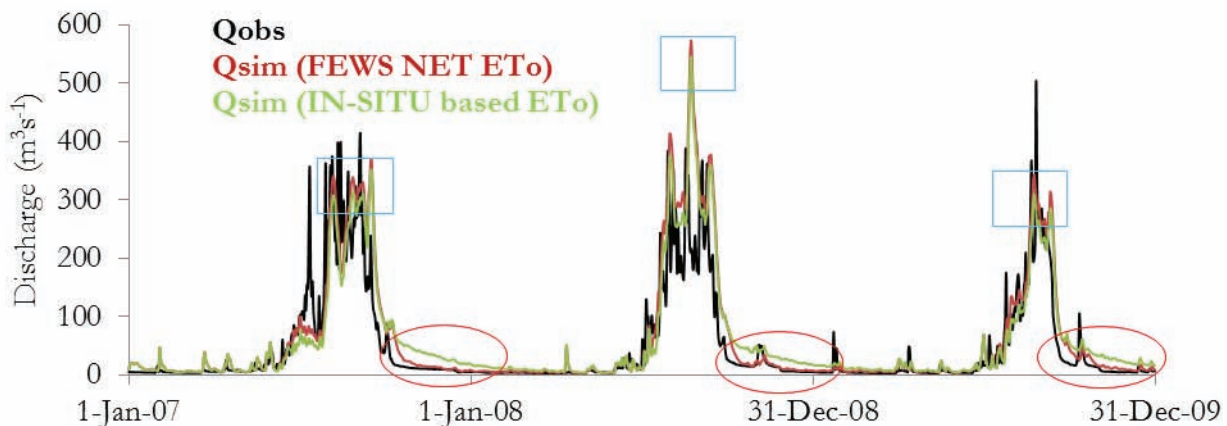


Figure 5-13: Comparison between observed and simulated hydrograph using FEWS NET and *in-situ* based ETo

5.7. Water level simulation for flood prone area(s) verification and onset of flooding

In this study, simulation of the water level at flood prone areas (see Figure 3-3) was done only to evaluate if the model is capable of simulating the increase of water level in the river channel and indicate the overtopping at those locations during the period of floods normally occurs (i.e. wet season: June to September). However, it is outside of the scope of this study to produce a flood depth or inundation map of the flood prone areas. To produce such maps, the following resources would be required.

- A hydrodynamic model which simulates flood depth and inundation at local scale;
- Detailed characteristics of the study area (like: the channel geometries, high resolution digital elevation model, etc);
- Hydrograph of observed hourly stream flow and detailed flood inundation maps that serve for model performance assessment.

Water level was simulated at the predicted flood prone locations for the years 2007-2009. Assuming a constant main river reach depth of 10 m, the simulation shows overtopping at those locations during every wet season (see Figure 5-14).

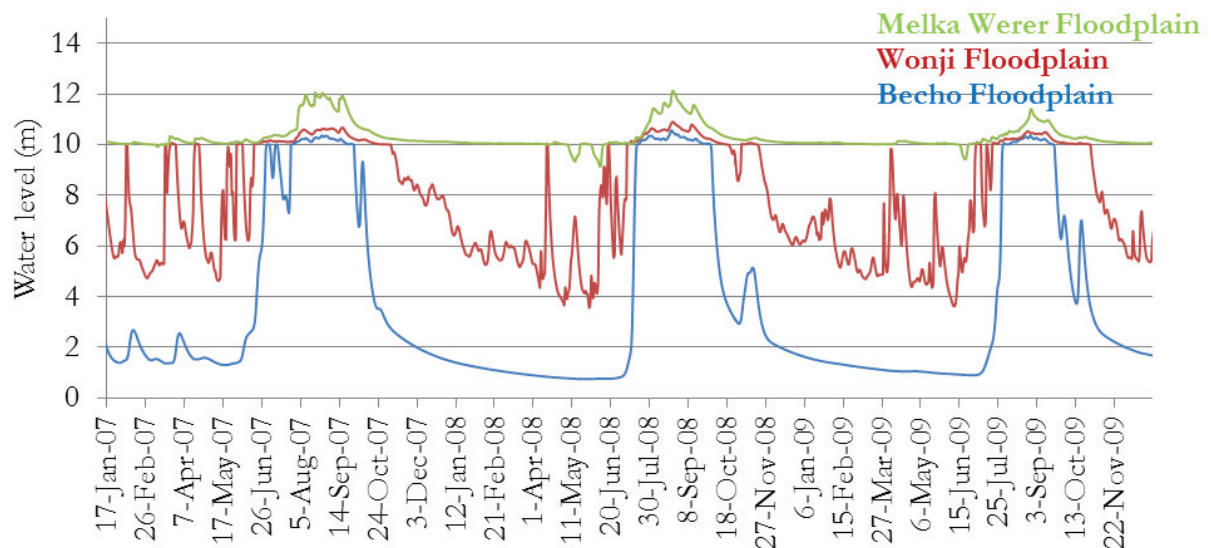


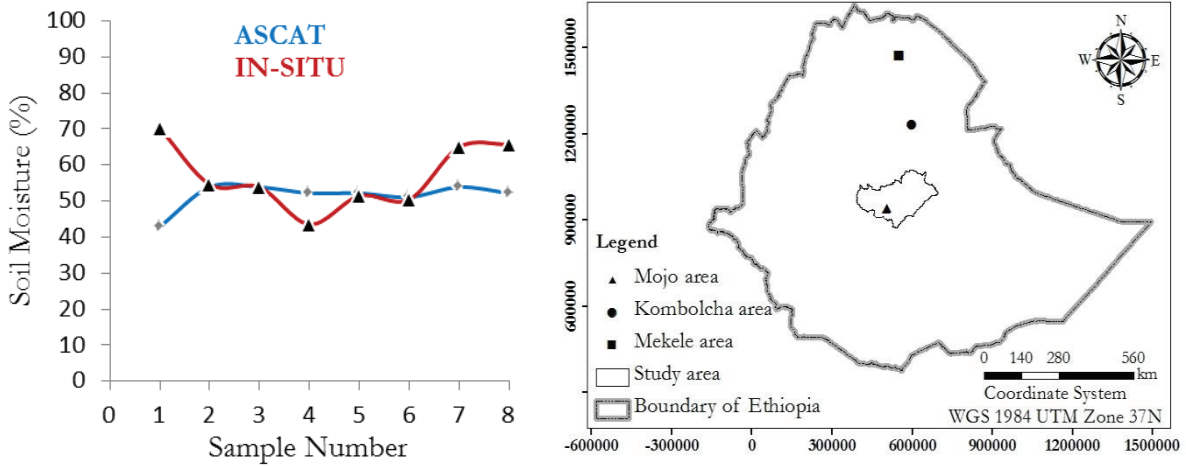
Figure 5-14: Water level simulation at the flood prone areas

5.8. ASCAT surface soil moisture to identify the wet pixel

The ASCAT surface soil moisture of 12.5km grid spacing was compared with *in-situ* measurements that were taken for two days at three sample areas in Ethiopia (see Figure 5-15(b)). The comparison was performed after the *in-situ* soil moisture is converted to saturation degree (0 – 100%), since the ASCAT surface soil moisture represents a dimensionless index between 0 and 100%. Assuming that 100% saturation degree from ASCAT is the same as the total porosity of the soil, the *in-situ* soil moisture (v/v) was converted to a saturation degree (0 – 100%).

Figure 5-15 (a) shows the comparison made at the Mojo sample area (located within the study area) and resulted in RMSE of 11.88% (~ 0.12). The result of 11.88% RMSE for the Mojo sample area indicates that the ASCAT surface soil moisture could be representative. The results from the other two sample areas (Kombolcha and Mekele) showed very poor correlation and were excluded from this study. There are several problems with using the ASCAT SSM products. The ASCAT sensor does not cover the entire study area with each satellite overpass (see Figure 5-16). Also, the temporal resolution of the sensor for

this study area is low (3-5 days). Moreover, Figure 5-16 (a) and (b) shows areas where the ASCAT surface soil moisture estimates are not available, even on places where there is overpass of the satellite. Therefore, due to the temporal and spatial limitation of the product for the study area, comparison of wetness distribution and flood affected areas was not done using this product (see Figure 5-16).



a) b)
Figure 5-15: Soil moisture validation result at Mojo area (a) and sample sites (b)

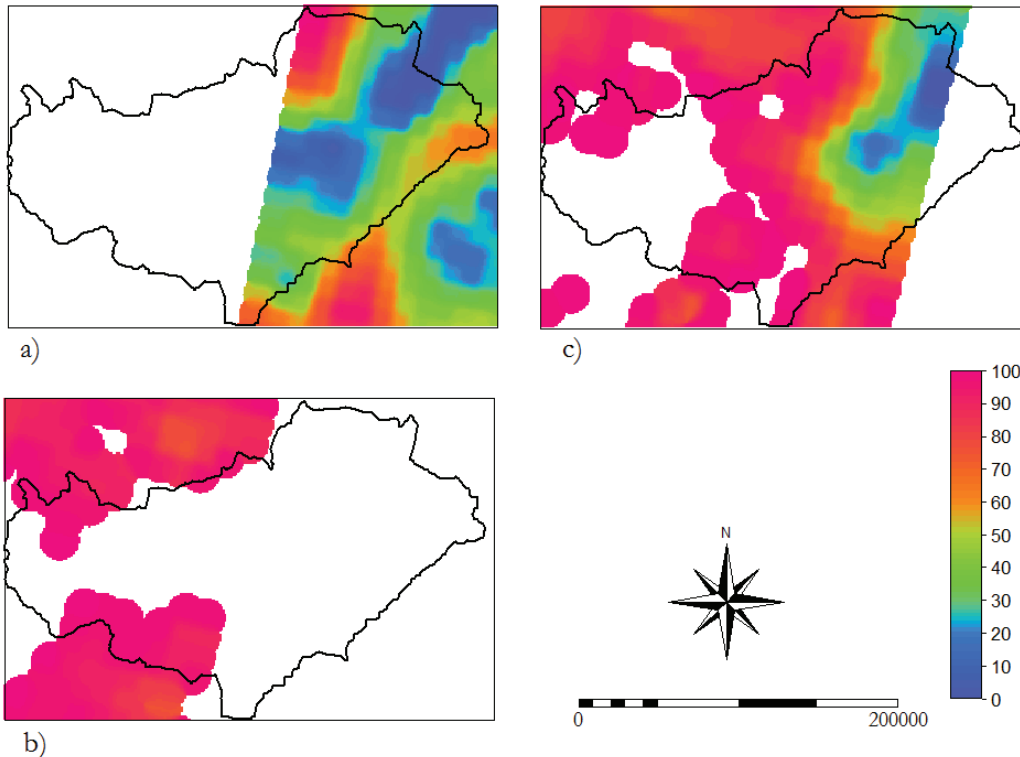


Figure 5-16: ASCAT surface soil moisture a) May 13, 2008; b) July 31, 2008; and c) July 7, 2008 day time overpasses

5.9. Analysis for Combining SPI and TWI

Three sample sites were selected to identify the time at which the daily SPI of the wet season (June – July) shows wet pixels (see Figure 5-17). The selections of the sites were done based on areas which were a possible cause of flooding in the flood prone areas.

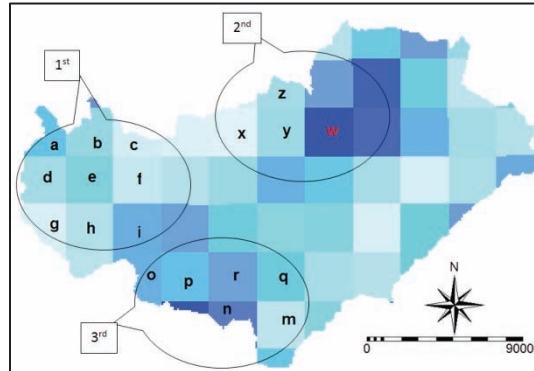


Figure 5-17: Locations where the SPI values of the wet season (June – August) were taken

Figure 5-18 shows the daily SPI variation of the 2007 wet season (June – August). As shown in Figure 5-18 there are two windows of time (June 13 – 20 and July 27 – August 04) that have high SPI values (>1). The two windows of time indicate the periods that the rainfall occurs which may cause flooding in flood prone areas. However, the rainfall during the first window (June 13 – 20) is less likely to be considered as a cause for riverine flooding in the catchment, because the time is close to the start of rainy season whereby the system (catchment) has less storage of moisture in the soil.

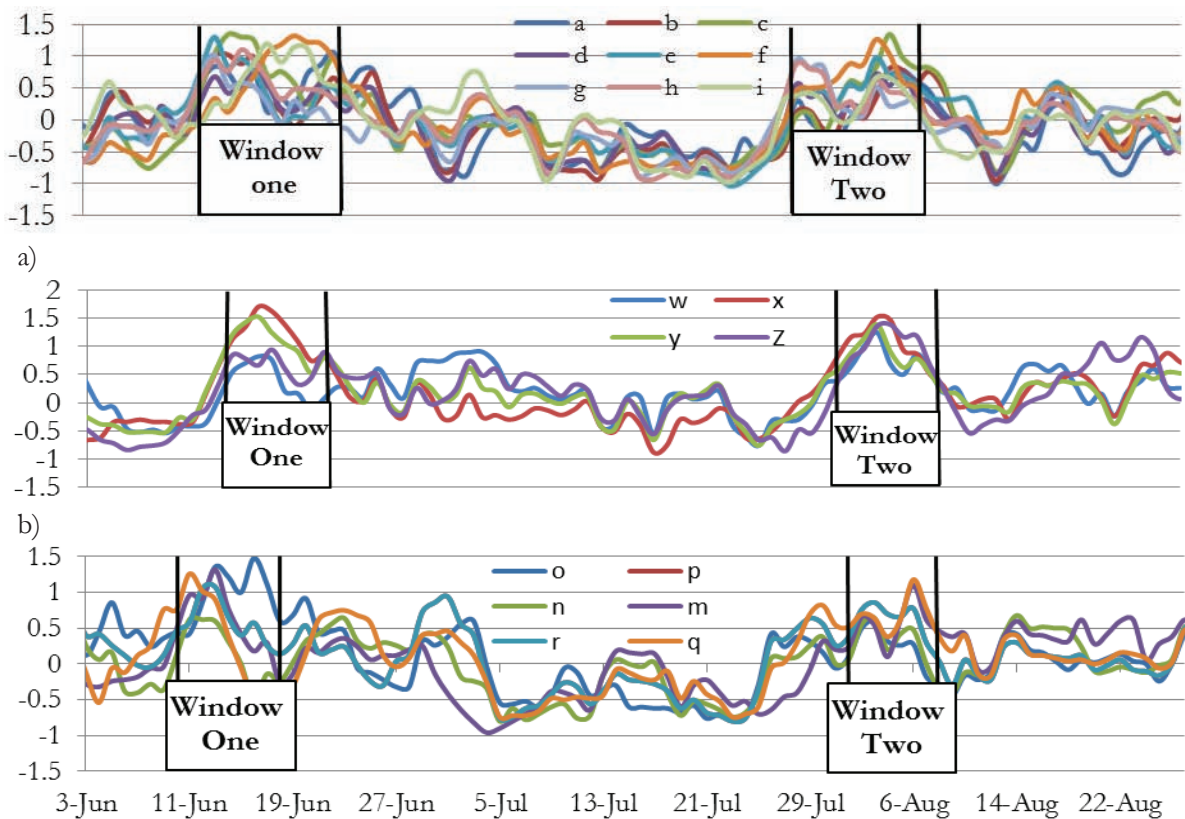
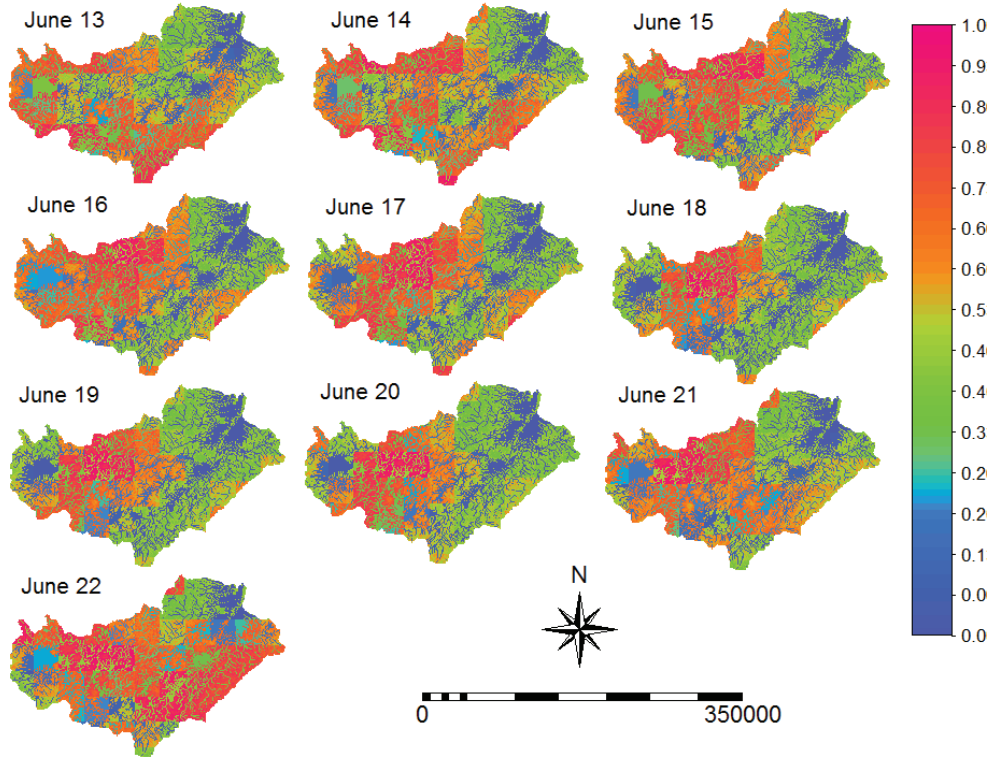
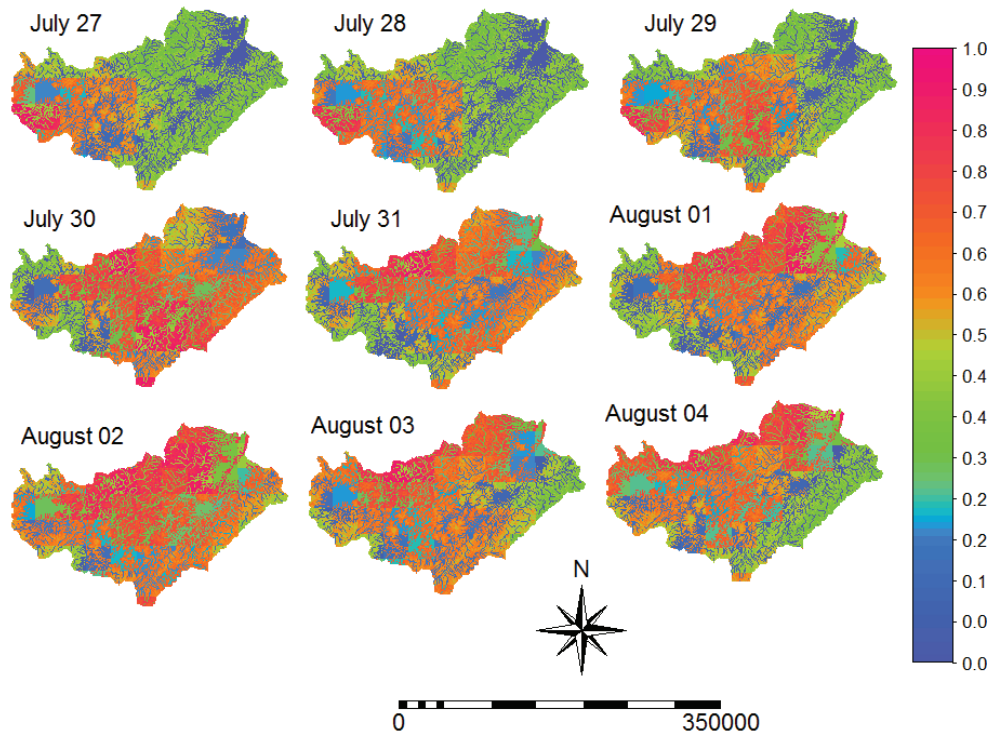


Figure 5-18: Temporal variation of wet season SPI: a) 1st site, b) 2nd site and c) 3rd site

Figure 5-19 below shows the spatial and temporal variation of the combined index during the two windows of time. The areas in pink-red indicate relatively high value areas while those areas in green-blue indicate relatively low value. Areas with high index values are considered source areas for flooding (peak flow) according to the combined index.



a)



b)

Figure 5-19: Combined index of 2007: a) window one and b) window two

5.10. Relation between water level and peak flow with SPI

From the simulated and/or observed hydrograph at Melka Hombole the highest peak flow occurred three times in 2007 (August 6 – 8, August 26 and September 16) and in 2008 (July 31, August 22 and September 11), whereas in 2009 was two times (August 24 and September 10) (see Figure 5-12). The highest water level observed at the flood prone areas in 2007 was during August 6 - 8, from August 20 – 23 and on September 6, while in 2008 and 2009 the highest water level observed was on August 22 and August 24 respectively (see Figure 5-14).

According to the information from Ethiopian MoWE (Hydrology department, oral communication) floods in the flood prone areas occur most of the time at the beginning of August (~1st to 8th), during third decade of August (~20th – 27th) and beginning of September (~1st – 5th). The incidence of floods during August (~1st to 8th) coincides with the time of peak flow in the river channel and high water level simulated of the period 2007. Furthermore, from the SPI analysis two windows of time (June 13 – 20 and July 27 – August 04) indicate the periods that the rainfall occurs which may cause flooding in flood prone areas (see Figure 5-18). Therefore, high SPI value (which indicates high rainfall above normal) during the second window of time can be attributed to the occurrence of the floods during the beginning of August, however, the result has to be further validated by applying local scale flood modelling.

6. CONCLUSIONS AND RECOMMENDATIONS

6.1. Summary and Conclusions

The main objective of this research is to evaluate if a flood early warning system for the upper and middle Awash River Basin located in Ethiopia could be developed by applying remote sensing based hydrological modelling. Simulation of stream flow of the upper and middle part of the Awash River Basin by LISFLOOD model for the period 2007-2009 was done using data from GEONETCast, Famine Early Warning System Network (FEWS NET), National Oceanic and Atmospheric Administration Climate Prediction Centre (NOAA CPC) and *in-situ* measurements. In the process several intermediary steps were performed. The sensitivity of LISFLOOD model to change in the calibration parameters was analysed. The LISFLOOD model was calibrated and validated. Satellite rainfall estimates and gauge measured rainfall were compared. Satellite based potential evapotranspiration estimates and *in-situ* based ETo estimates were compared. The effect of *in-situ* based and FEWS NET ETo on the LISFLOOD simulation hydrograph was investigated. Water level simulation was simulated. ASCAT surface soil moisture was validated. The standard precipitation index was analysed. Finally the combined index using SPI and TWI were produced.

The sensitivity of five LISFLOOD parameters was performed. According to the result from the sensitivity analysis, the LZTC and GWPV parameters showed effect on the base flow part of the hydrograph. An increase in the LZTC parameter value resulted in the decrease in the flow from the lower zone groundwater store, since it is related inversely to the discharge from the lower zone groundwater in the model. An increase in the GWPV parameter value resulted in an increase in base flow and decrease in the peak flow parts of the hydrograph, as the parameter controls the flow from the upper to the lower zone groundwater store. When there is high percolation (high GWPV) to the lower zone groundwater store from the upper zone groundwater store, the amount of water available for quick flow decreases which leads to decrease in peak flow and the amount of low flow increases which leads to high base flow (see Figure 5-8). Whereas, as observed from the sensitivity result most of the effects of the other three parameters (UZTC, PPBF and Xb) are on the quick flow. As the UZTC parameter value increases the peak flow decreases and the slope of the recession limb becomes gentler. This is because the parameter is formulated in such a way that it is inversely proportional to the discharge from the upper zone groundwater store. The PPBF value of 1 showed an unrealistic response of the catchment where by the soil matrix captures no rainfall and water is immediately discharged from the catchment (see Figure 5-10). This could indicate that the parameter values should not be less than 5 as was suggested by Feyen et al., (2007).

After applying two year warm-up period, the model was calibrated by trial and error using the observed stream flow from 2007 and 2008 and validated using 2009. The final simulation result showed that in 2008 the simulated peak flow is higher than the observed peak flow, whereas in 2009 the observed peak flow is higher than the simulated peak flow (probably be due to wrong measurement). Furthermore, the simulation result in 2007 does not fit the first peak in the observed stream flow hydrograph. For the calibration period RMSE = $55.29\text{m}^3\text{s}^{-1}$, NSE = 0.72 and RVe = 0.27% and for validation period RMSE = $29.37\text{m}^3\text{s}^{-1}$, NSE = 0.82 and RVe = 21.07% were obtained.

Satellite rainfall estimate products CMORPH (2006 – 2010) and MPE (2010) were compared to gauge measured rainfall. The CMORPH annual rainfall estimates were lower than the measured rainfall at all

stations except Abomsa, Gelemso, Miesso and Ziway for the period 2007 and Gelemso and Miesso for the period 2009. The average annual difference (12 stations) is $246\text{mm}\text{yr}^{-1}$ for CMORPH and $669\text{mm}\text{yr}^{-1}$ for MPE. MPE has a larger underestimation than CMORPH. Moreover, MPE quality analysis by Samain and Heinemann (2007) indicated that MPE product is not suitable to locate rain-pattern correctly for the study area, since correlation between IR derived rain rate and the SSM/I rain rate is very low.

The ETo estimates using *in-situ* measured meteorological variables and the FEWS NET ETo estimates using Global Data Assimilation System meteorological variables were compared. The FEWS NET ETo estimates during wet seasons are underestimated compared to *in-situ* based ETo estimates, whereas, the average annual accumulated ETo from FEWS NET is 64mm higher than the *in-situ* based ETo. The average RMSE found was $1.2\text{mm}\text{day}^{-1}$ for 2006 - 2010 periods.

The Awash River stream flow simulation using satellite based ETo (FEWS NET) and *in-situ* based ETo was done for the period of 2007 – 2009. The result shows that the peak flow decreases and the recession part of the base flow increases when the *in-situ* based ETo was used as a forcing term. The higher peak flow for FEWS NET ETo is probably due to the underestimation of FEWS NET ETo during the wet season. A lower ETo estimate results in lower extraction of water from the catchment which leads to higher peak flow for FEWS NET. The lower estimate for the peak flow using *in-situ* based ETo leads to a delay in the discharge response, which in turn leads to a higher base flow in the recession part of the hydrograph.

Three sample sites were selected to identify the time at which the daily SPI of the wet season (June – July) shows wet pixels. From the analysis of the daily SPI values of the wet period, two windows of time (June 13 – 20 and July 27 – August 04) were found that have high SPI values (>1). The two windows of time indicate the periods that the rainfall occurs which may cause flooding in flood prone areas. However, the rainfall during the first window (June 13 – 20) is less likely to be considered as a cause for riverine flooding in the catchment, because the time is close to the start of rainy season when the system (catchment) has less storage of moisture in the soil. However, to identify when the floods can be caused during the second window needs further study. Such would require the application of the LISFLOOD model or another hydrodynamic model which simulates flood depth and inundation at the local scale. Furthermore, detailed characteristics of the study area (like the river channel geometries, high resolution digital elevation model, etc), a hydrograph of observed hourly stream flow and detailed flood inundation maps that serve for model performance assessment are required.

From the simulation of the discharge and water level in the river channel, the time at which the peak flow (around August 6 - 8) and high water level (around August 6 - 8) occurred corresponds with the time of flooding in the flood prone areas (around August 1 - 8). Furthermore, from the SPI analysis two windows of time (June 13 – 20 and July 27 – August 04) indicate the periods that the rainfall occurs which may cause flooding in flood prone areas (see Figure 5-18). Therefore, high SPI value (which indicates high rainfall above normal) during the second window of time can be attributed to the occurrences of the floods during the beginning of August, however, the result has to be further validated by applying local scale flood modelling.

The ASCAT 12.5km grid spacing surface soil moisture product was compared with *in-situ* measurements taken for two days at three sample areas in Ethiopia. The result of 11.88% (~ 0.12) RMSE for the Mojo sample area indicates that the ASCAT surface soil moisture could be representative. However, the results from the other two sample areas (Kombolcha and Mekele) showed very poor correlation and were excluded from this study. There are several problems with using the ASCAT SSM products. The ASCAT sensor does not cover the entire study area with each satellite overpass. Also, the temporal resolution of

the sensor for this study area is low (3-5 days). Moreover, Figure 5-16 shows areas where the products do not give surface moisture values. Therefore, due to the temporal and spatial limitation of the product for the study area, comparison of wetness distribution and flood affected areas was not done using this product.

To summarize:

- LISFLOOD is sensitive to the five parameters used for calibration (UZTC, LZTC, GWPV, Xb and PPBF).
- The performance of LISFLOOD to simulate stream flow is largely governed by the meteorological forcing terms (especially; rainfall).
- The CMORPH and MPE rainfall estimates are lower than *in-situ* observed rainfall for upper and middle Awash River Basin.
- FEWS NET ETo estimates during wet seasons are underestimated compared to *in-situ* based ETo estimates, whereas, the average annual accumulated ETo from FEWS NET is 64mm higher than the *in-situ* based ETo.
- Given the limited reliability of the observed stream flow, the LISFLOOD model was calibrated using trial and error calibration. For the calibration period RMSE = 55.29m³s⁻¹, NSE = 0.72 and RVe = 0.27% and for validation period RMSE = 29.37m³s⁻¹, NSE = 0.82 and RVe = 21.07% were obtained at Melka Hombole station.
- Water level simulation shows overtopping at flood prone area during every wet season (June – July).
- According to the SPI analysis, the rainfalls during two windows of time within the wet season (June 13 – 20 and July 27 – August 04) are the main cause for floods in the flood prone areas.
- The combined index analysis illustrated the spatial distribution of possible source areas for floods in the flood prone areas.

6.2. Recommendations

- In this study the effect of dams (Koka and Kessem), sugar factories (Wonji-Shoa and Matahara), and a number of small and large scale irrigation systems which exist in the study area were not considered. To come up with a better simulation of the Awash River flow, estimation of the water extracted by the irrigation schemes and the sugar factories are necessary. In addition, the effect of the dams in relation to flooding in the area needs to be studied.
- The comparison of the satellite based rainfall estimate with the gauge measured rainfall was done only on annual rainfall totals at each station with visual interpretations and simple statistics (the annual cumulative difference). Further statistical measures of fit have to be applied by considering more stations and a longer period of rainfall records.
- The SPI computation is only limited to 5 years of rainfall records and needs further validation, so additional analysis is required that considers longer time rainfall records.
- The application of LISFLOOD in flood prone areas at local scale is necessary to simulate historic flood events and to know the exact onset of flooding.

LIST OF REFERENCES

- Abraha, A. A. (2006). Flood Modelling and Forecasting for Awash River Basin in Ethiopia. MSc. Thesis, UNESCO-IHE Institute, Delft, Netherlands.
- Achamyeleh, K. (2003). The Associated Programme on Flood Management; Integrated Flood Management, Case Study Ethiopia: WMO and GWP. Available at: http://www.apfm.info/pdf/case_studies/cs_ethiopia.pdf, last Retrieved 2011-Aug-25.
- Albergel, C., de Rosnay, P., Gruhier, C., Muñoz-Sabater, J., Hasenauer, S., Isaksen, L., . . . Wagner, W. (2012). Evaluation of Remotely Sensed and Modelled Soil Moisture Products Using Global Ground-based In-situ Observations. *Remote Sensing of Environment*, 118(0), 215-226.
- Alemayehu, Z. (2007). Modelling of Flood Hazard Management for Forecasting and Emergency Response of 'Koka' Area within Awash River Basin Using Remote sensing and GIS method. MSc. Thesis, Addis Ababa University, Addis Ababa, Ethiopia.
- Allen, R. G., Pereira, L. S., Raes, D. and Smith, M. (1998). Crop Evapotranspiration - Guidelines for Computing crop water requirements - FAO. Irrigation and Drainage Paper 56, FAO Rome.
- Allen, R. G., Pruitt, W. O., Raes, D., Smith, M., & Pereira, L. S. (2005). Estimating evaporation from bare soil and the crop coefficient for the initial period using common soils information. *Journal of Irrigation and Drainage Engineering-Asce*, 131(1), 14-23.
- Anderson, M. G. Burt, T. P. (1985). Modelling Strategies. M. G. Anderson & T. P. Burt (Eds.), *Hydrological Forecasting* (pp. 1-13). New York: John Wiley & Sons.
- Arnold, J. G. Fohrer, N. (2005). SWAT2000: Current Capabilities and Research Opportunities in Applied Watershed Modelling. *Hydrological Processes*, 19(3), 563-572.
- Bartalis, Z., Naeimi, V., Hasenauer, S., Wagner, W. (2008). ASCAT Soil Moisture Product Handbook. ASCAT Soil Moisture Report Series, No. 15, Institute of Photogrammetry and Remote Sensing, Vienna University of Technology, Austria. Available at: http://www.ipf.tuwien.ac.at/radar/ascats/report_series/15_ASCAT%20Soil%20Moisture%20Product%20Handbook_v1.3.pdf, last retrieved 2011-Aug-27.
- Beven, K. J. (2003). Rainfall-runoff Modelling: *The Primer*. West Sussex, John Wiley & Sons.
- Beven, K. J. Kirkby, M. J. (1979). A Physically Based, Variable Contributing Area Model of Basin Hydrology. *Hydrological Sciences Bulletin*, 24(1), 43-69.
- Billa, L., Mansor, S., Mahmud, A. R., & Ghazali, A. H. (2006). Modelling Rainfall Intensity from NOAA AVHRR Data for Operational Flood Forecasting in Malaysia. *International Journal of Remote Sensing*, 27(23), 5225-5234.
- Brocca, L., Melone, F., Moramarco, T., Wagner, W., & Hasenauer, S. (2010). ASCAT Soil Wetness Index Validation Through In-situ and Modeled Soil Moisture Data in Central Italy. *Remote Sensing of Environment*, 114(11), 2745-2755.
- Budhakooncharoen, S. (2004). Rainfall Estimate for Flood Management Using Meteorological data from satellite imagery. *9th Biennial International Conference on Engineering, Construction and Operations in Challenging Environment*, League City Houston, USA.
- Burger, G., Reusser, D., & Kneis, D. (2009). Early Flood Warnings from Empirical (expanded) Downscaling of The Full ECMWF Ensemble Prediction System. *Water Resources Research*, vol. 45, 15 pages.

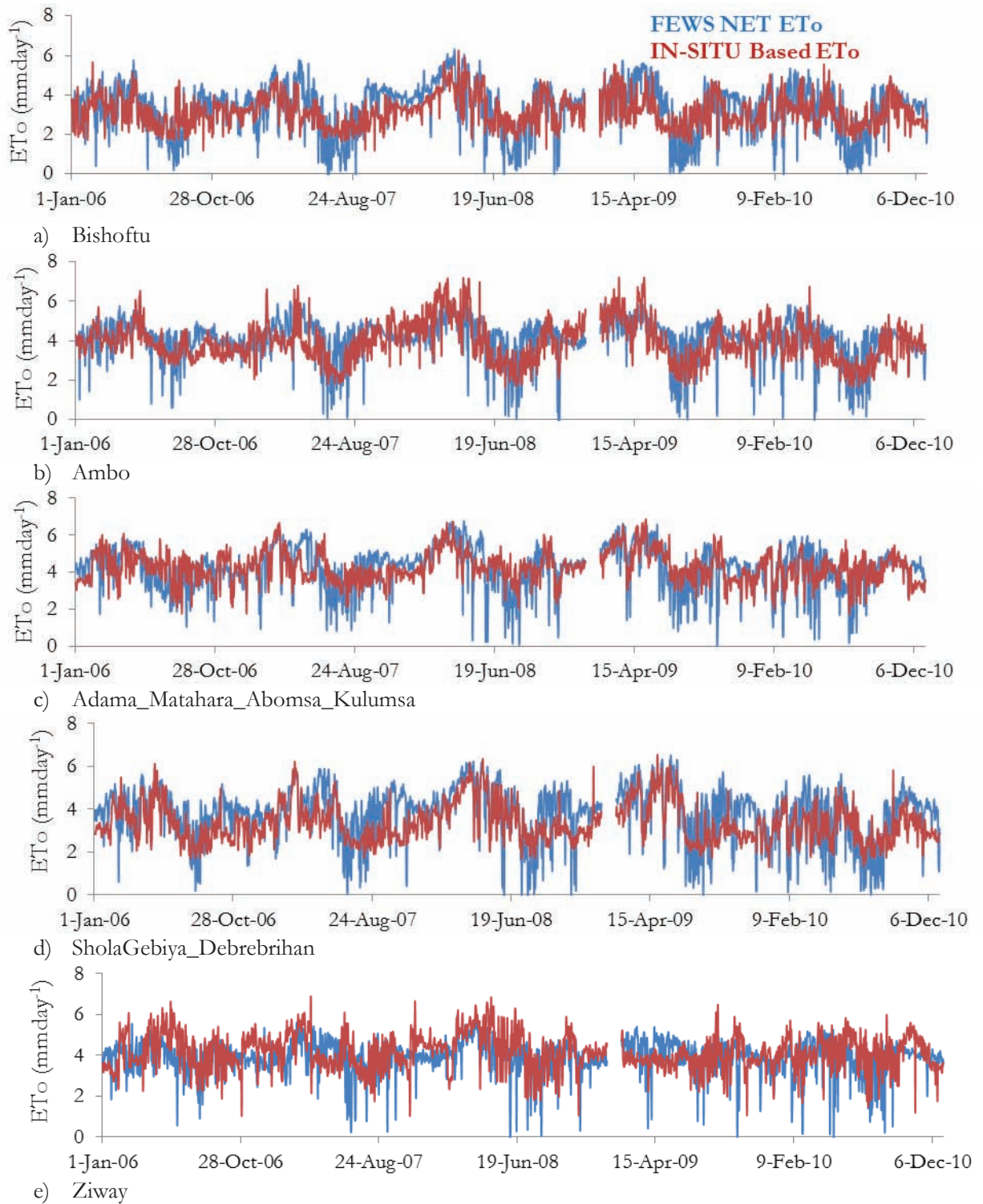
- CGIAR-CSI. (2011). SRTM 90m Digital Elevation Database v4.1. Available at: <http://srtm.csi.cgiar.org/> (accessed 2011-Oct-12).
- Dankers, R., Christensen, O. B., Feyen, L., Kalas, M., & de Roo, A. (2007). Evaluation of Very High-Resolution Climate Model Data for Simulating Flood Hazards in The Upper Danube Basin. *Journal of Hydrology*, 347(3-4), 319-331.
- De Roo, A., Schmuck, G., Perdigao, V., & Thielen, J. (2003). The Influence of Historic Land Use Changes and Future Planned Land Use Scenarios on Floods in The Oder Catchment. *Physics and Chemistry of the Earth, Parts A/B/C*, 28(33-36), 1291-1300.
- De Roo, A. P. J., Wesseling, C. G., & Van Deursen, W. P. A. (2000). Physically Based River Basin Modelling within a GIS: The LISFLOOD Model. *Hydrological Processes*, 14(11-12), 1981-1992.
- ESIG ALERT. (2004). Early Warning Systems and Sustainable Development. *Early Warning Systems Do's and Don'ts conference (2003-oct-20-23)*. Available at: <http://www.isse.ucar.edu/alerts/alert6.html>, last retrieved 2012-Jan-02.
- EUMETSAT. (2011). MSG Meteorological Products Extraction Facility Algorithm Specification Document. Darmstadt, Germany. Available at: http://www.eumetsat.int/groups/ops/documents/document/PDF_TEN_SPE_04022_MSG_MPEF.pdf, last retrieved 2012-Jan-10.
- FAO. (2001). Lecture Notes on the Major Soils of the World. In Paul Driessen & Jozef Deckers (Eds.) *FAO Corporate Document Repository database*. Available at: <http://www.fao.org/DOCREP/003/Y1899E/Y1899E00.HTM>, last retrieved 2011-Dec-10.
- FEWS NET. (2011). Famine Early Warning System Network, Global Potential Evapotranspiration (PET). Available at: <http://earlywarning.usgs.gov/fews/global/web/readme.php?symbol=pt>, (accessed 2011- Nov -30).
- Feyen, L., Vrugt, J. A., Nualláin, B. Ó., van der Knijff, J., & De Roo, A. (2007). Parameter Optimisation and Uncertainty Assessment for Large-scale Streamflow Simulation with The LISFLOOD Model. *Journal of Hydrology*, 332(3-4), 276-289.
- ADB. (2011). Awash River Flood Control Study. Available at: <http://www.afdb.org/en/projects-and-operations/project-portfolio/project/p-et-aac-010/>, (accessed 2011-Aug-10).
- Hoefsloot, P. (2010). LEAP version 2.4 for Ethiopia User manual. Available at: <http://www.hoefsloot.com/en/leap-for-ethiopia>, (accessed 2010-May-20).
- Halcrow. (2006). Awash River Basin Flood Control and Watershed Management Study Project. Halcrow and MoWE, Addis Ababa, Ethiopia.
- Joyce, R. J., Janowiak, J. E., Arkin, P. A., & Xie, P. (2004). CMORPH: A Method that Produces Global Precipitation Estimates from Passive Microwave and Infrared Data at High Spatial and Temporal Resolution. *Journal of Hydrometeorology*, 5(3), 487-503.
- Laguardia, G., Niemeyer, S. (2008). On the comparison between the LISFLOOD modelled and the ERS/SCAT derived soil moisture estimates. *Hydrology and Earth System Sciences*, 12(6), 1339-1351.
- SAF, L. (2011). The EUMETSAT Satellite Application Facility on Land Surface Analysis (LSA SAF) Product User Manual on Vegetation Parameters (FVC, LAI, FAPAR). Available at <http://landsaf.meteo.pt/algorithms.jsp?seltab=9&starttab=7>, last retrieved 2011-Oct-01.
- Maathuis, B. H. P., Mannaerts, C. M., Schouwenburg, M., Retsios, V. and Lemmens, R. L. G. (2011b). GEONETCast Toolbox: Installation, Configuration and User Guide of the GEONETCast

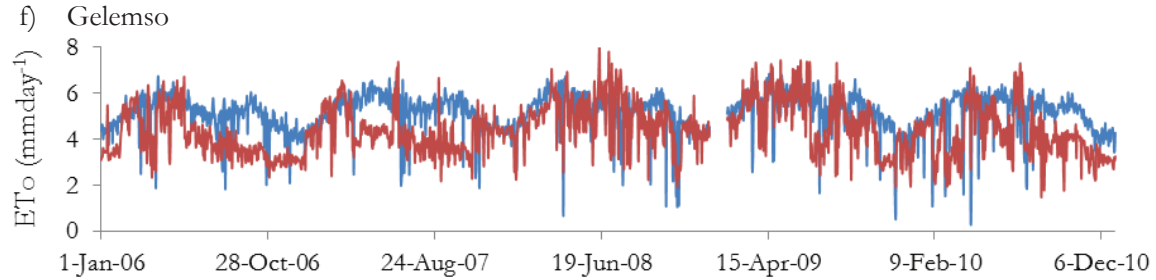
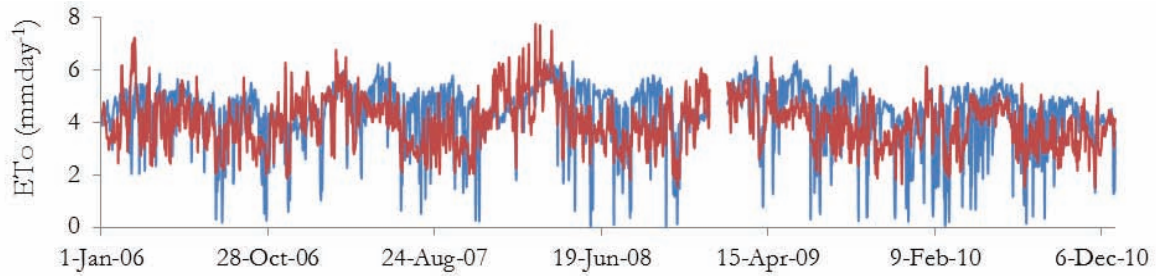
- TOOLBOX Plug-in for ILWIS 3.7: ITC, Enschede, the Netherlands. 2011. Available at: <http://52north.org/downloads/earth-observation/geonetcast/toolbox>, last retrieved 2011-Aug-20.
- Maathuis, B. H. P. Wang, L. (2006). Digital Elevation Model Based Hydro-processing. Hong Kong: *Geocarto International Centre*. Available at: http://www.geocarto.com.hk/cgi-bin/pages1/mar06/3_Maathuis.pdf, last retrieved 2011-Nov-20.
- Maidment, D. R. (1992). *Handbook of Hydrology*. United States: McGraw-Hill.
- Mannaerts, C. M. Maathuis, B. H. P. (2011). Use of GEONETCast Real Time Satellite Data Streams for Water and Food Security Early Warning. *WFP-ITC project workshop 20 June - 1 July 2011*. Available at: <http://www.itc.nl/Pub/Events-Conferences/2011/June2011/WFP-ITC-workshop-GEONETCast.html> (accessed 2011-August-12).
- McKee, T. B., Doesken, N. J., Kleist, J., & Amer Meteorol, S. O. C. (1993). The Relationship of Drought Frequency and Duration to time scales. *The 8th Conference on Applied Climatology*. Available at: <http://ccc.atmos.colostate.edu/relationshipofdroughtfrequency.pdf>, last retrieved 2012-Jan-10.
- Moriasi, D. N., Arnold, J. G., Van Liew, M. W., Bingner, R. L., Harmel, R. D., & Veith, T. L. (2007). Model Evaluation Guidelines for Systematic Quantification of Accuracy in Watershed Simulations. *Transactions of the Asabe*, 50(3), 885-900.
- MoWE. (2011). Nature and Features of The Ethiopian River Basins. Ministry of Water and Energy. Available at: <http://www.mowr.gov.et/index.php?pagenum=3.1&pagehgt=5500px>, last retrieved 2011-Aug-15.
- NASA. (2011). Flooding Along the Awash River in Ethiopia. *Earth Observatory*. Available at: <http://earthobservatory.nasa.gov/NaturalHazards/view.php?id=12065>, last retrieved 2011-Aug-16.
- Neitsch, S. L., Arnold, J. G., Kiniry, J. R., Srinivasan, R., & Williams, J. R. (2002). Soil and Water Assessment Tool User's Manual (Version 2000). *Texas Water Resources Institute*. Available at: <http://www.brc.tamus.edu/swat/downloads/doc/swatuserman.pdf>, last retrieved 2011-Aug-20.
- Penman, H. L. (1948). Natural Evaporation from Open Water, Bare Soil and Grass. *Proceedings of the Royal Society of London. Series A, Mathematical and Physical Sciences*, 193(1032), 120-145.
- Rawls, W., D. Brakensiek, et al. (1982). Estimation of Soil Water Properties. *American Society of Agricultural Engineers*, Vol. 25, No. 5. Pp. 1316-1320 & 1328.
- Rientjes, T. H. M. (2004). Inverse Modelling of The Rainfall - Runoff Relation : A Multi Objective Model Calibration Approach. PhD THESIS, Delft University Press, Delft.
- Salamon, P. Feyen, L. (2009). Assessing Parameter, Precipitation, and Predictive Uncertainty in a Distributed Hydrological Model Using Sequential Data Assimilation with The Particle Filter. *Journal of Hydrology*, 376(3-4), 428-442.
- Samain, O. Heinemann, T. (2007). MPE Quality indicators. Darmstadt, Germany: EUMETSAT. Available at: http://www.eumetsat.int/groups/ops/documents/document/pdf_metprod_mpe_quality_info.pdf, last retrieved 2012-Jan-10.
- Scharffenberg, W. A. (2008). HEC-HMS Model Overview. *The Technical Workshop on Watershed Modelling with HEC-HMS*. Available at: <http://www.cwemf.org/workshops/HEC-HMSwrkshp/HEC-HMSWrkshp.pdf>, last retrieved 2011-Aug-25.

- Scharffenberg, W. A., Fleming, M. J., & Hydrologic Engineering, C. (2006). Hydrologic modelling system HEC-HMS: user's manual. Davis, CA: US Army Corps of Engineers, Hydrologic Engineering Center. Available at: http://www.hec.usace.army.mil/software/hec-hms/documentation/CPD-74A_2001Jan.pdf, last retrived 2011-Aug-22.
- Taddese G., Sonder K., & D., P. (2006). The Water of the Awash River Basin a Future Challenge to Ethiopia. *International Livestock Research Institute (ILRI)*. Addis Ababa, Ethiopia. Available at: <http://www.iwmi.cgiar.org/assessment/files/pdf/publications/WorkingPapers/WaterofAwasBasin.pdf>, last retrieved 2011-Nov-10.
- Thiemig, V., de Roo, A., & Gadain, H. (2011). Current Status on Flood Forecasting and Early Warning in Africa. *International Journal of River Basin Management*, 9(1), 63-78.
- Thiemig, V., Pappenberger, F., Thielen, J., Gadain, H., de Roo, A., Bodis, K., . . . Muthusi, F. (2010). Ensemble Flood Forecasting in Africa: a Feasibility Study in The Juba-Shabelle River Basin. *Atmospheric Science Letters*, 11(2), 123-131.
- UNISDR. (2009). UNISDR Terminology on Disaster and Risk Reduction. *UN International Strategy for Disaster Reduction*; Geneva, Switzerland. Available at: http://www.unisdr.org/files/7817_UNISDRTerminologyEnglish.pdf, last retrieved 2011-Nov-12.
- Guinand, Y., (1999). UNDP-EUE: Afar Region - Awash River Floods, 09/99. *UNDP Emergencies Unit of Ethiopia*. Available at: <http://www.africa.upenn.edu/Hornet/afar0999.html>, (accessed 2011-Aug-20).
- Van der Knijff, J. and A. De Roo (2008). LISFLOOD Distributed Water Balance and Flood Simulation Model. Revised User Manual. *Joint Research Centre, European Commision*, Luxembourg. ISSN 1018-5593: 109.
- Van Deursen, W. P. A. Wesseling, C. G. (1991). Introduction to the PCRaster Package: Concepts, Package Layout. PCRaster Version 2 Manual. Available at: <http://pcraster.geo.uu.nl/documentation/pcrman/book1.htm>, last retrieved 2011-Dec-31.
- WMO. (2009). Integrated Flood Management; Concept Paper. *World Meteorological Organization*, Geneva, Switzerland. Available at: Retrieved from URL http://www.apfm.info/pdf/concept_paper_e.pdf, last retrieved 2011-Agust-26.

ANNEX

D) Daily variation of FEWS NET and *in-situ* based ETo estimates (2006 – 2007)





g) Miesso

II) Annual FEWS NET and *in-situ* based ETo estimates at respective station for the year 2006, 2008, 2009 and 2010

